



Anti-Icing and De-icing Superhydrophobic Concrete to Improve the Safety on Critical Elements of Roadway Pavements

CFIRE 07-03
September 2013

National Center for Freight & Infrastructure Research & Education
Department of Civil and Environmental Engineering
College of Engineering
University of Wisconsin–Madison



Authors:

Konstantin Sobolev, Michael Nosonovsky,
Ismael Flores-Vivian, Sunil Rao, Marina
Kozhukhova, Vahid Hejazi, Scott Muzenski,
Brandon Bosch, Rossana Rivero
University of Wisconsin - Milwaukee

Tom Krupenkin
University of Wisconsin – Madison

Principal Investigators:

Konstantin Sobolev (PI),
Michael Nosonovsky (co-PI)
University of Wisconsin – Milwaukee

Tom Krupenkin (co-PI)
University of Wisconsin – Madison

DISCLAIMER

This research was funded by the National Center for Freight and Infrastructure Research and Education. The contents of this report reflect the views of the authors, who are responsible for the facts and the accuracy of the information presented herein. This document is disseminated under the sponsorship of the Department of Transportation, University Transportation Centers Program, in the interest of information exchange. The U.S. Government assumes no liability for the contents or use thereof. The contents do not necessarily reflect the official views of the National Center for Freight and Infrastructure Research and Education, the University of Wisconsin-Milwaukee, the University of Wisconsin-Madison, the Wisconsin Department of Transportation, or the USDOT's RITA at the time of publication.

The United States Government assumes no liability for its contents or use thereof. This report does not constitute a standard, specification, or regulation.

The United States Government does not endorse products or manufacturers. Trade and manufacturers names appear in this report only because they are considered essential to the object of the document.

1. Report No. CFIRE 07-03	2. Government Accession No.	3. Recipient's Catalog No. CFDA 20.701	
4. Title and Subtitle Anti-Icing and De-Icing Superhydrophobic Concrete to Improve the Safety on Critical Elements on Roadway Pavements		5. Report Date September 2013	
		6. Performing Organization Code	
7. Author/s Konstantin Sobolev, Michael Nosonovsky, Tom Krupenkin , Ismael Flores-Vivian, Sunil Rao, Marina Kozhukhova, Vahid Hejazi, Scott Muzenski, Brandon Bosch, Rossana Rivero		8. Performing Organization Report No. CFIRE 07-03	
9. Performing Organization Name and Address National Center for Freight and Infrastructure Research and Education (CFIRE) University of Wisconsin-Madison 1415 Engineering Drive, 2205 EH Madison, WI 53706		10. Work Unit No. (TR AIS)	
		11. Contract or Grant No. 432k364	
12. Sponsoring Organization Name and Address Research and Innovative Technology Administration United States Department of Transportation 1200 New Jersey Ave, SE Washington, D.C. 20590		13. Type of Report and Period Covered	
		14. Sponsoring Agency Code	
15. Supplementary Notes Project completed for the USDOT's RITA by CFIRE.			
16. Abstract Icy roads lead to treacherous driving conditions in regions of the U.S. resulting in over 450 fatalities per year. De-icing chemicals, such as rock salt help to reduce ice formation on roadways to an extent, however also result in detrimental effects to concrete and especially reinforced concrete. The creation of an icephobic concrete can provide a much extended lifespan for critical elements of bridges and other transportation infrastructure. Moreover, the use of icephobic materials in highway infrastructure can significantly reduce the need for maintenance. With increasing costs for de-icing and anti-icing materials currently used on highways, and considering new environmental regulations, the need for new icephobic cementitious composites which can provide the required durability and mechanical response for critical elements of transportation infrastructure is evident. In this research, superhydrophobic siloxane admixtures were applied to concrete surfaces rendering them icephobic. These superhydrophobic admixtures were developed and investigated to reduce the ice adhesion to concrete surfaces. In addition, the proposed method involves the engineering of the hierarchical structure for concrete wearing surface by optimization of aggregates and the use of fibers. The research demonstrated that the best water repellent materials (measured by the contact angle) were obtained using polymethyl-hydrogen-siloxane. The addition of fibers and the dilution of the emulsion were found to be the parameters that greatly enhance the hydrophobicity. Diluted emulsions (5% active material) allow the fiber to produce a hierarchical surface of fibers and aggregates so the material has superhydrophobic properties.			
17. Key Words de-icing, concrete, icephobic, hydrophobic, overhydrophobic, superhydrophobic, treatment, ice adhesion		18. Distribution Statement No restrictions. This report is available through the Transportation Research Information Services of the National Transportation Library.	
19. Security Classification (of this report) Unclassified	20. Security Classification (of this page) Unclassified	21. No. Of Pages 39	22. Price -0-

Form DOT F 1700.7 (8-72)

Reproduction of form and completed page is authorized.

TABLE OF CONTENTS

1. INTRODUCTION	1
1.1 HYDROPHOBICITY AND SUPERHYDROPHOBICITY	4
1.2 HYDROPHOBIC COATINGS ON CONCRETE BASED MATERIALS	4
1.2.1 WATERPROOFING TREATMENTS.	4
1.2.2 HYDROPHOBIC ADMIXTURE TREATMENTS	7
2. DEVELOPING THE ICEPHOBIC PROPERTIES	8
2.1 CHEMICAL COMPOSITION	8
2.2 APPLICATION METHODS	9
2.3 TESTING PROCEDURES	10
3. RESEARCH OBJECTIVES	12
3.1 MATERIALS AND EXPERIMENTAL PROCEDURES	12
3.1.1 MORTAR MATERIALS	12
3.1.2 PROPORTIONS OF PORTLAND CEMENT MORTARS	13
3.1.3 TYPE AND PREPARATION OF SPECIMENS	13
3.1.4 PRELIMINARY STUDY – SCREENING OF SILANE AND SILOXANE COMPOUNDS	13
3.1.5 EMULSION MATERIALS	14
3.1.6 EMULSION PREPARATION	15
3.2 TYPE AND PREPARATION OF SPECIMENS	17
3.2.1 EMULSION TYPE EFFECT	17
3.2.2 MORTAR ROUGHNESS AND EMULSION DOSAGE EFFECT	17
3.2.3 SPLITTING TEST FOR ICE ADHESION	17
3.2.4 HYDROPHOBICITY AND ICEPHOBICITY TESTING	19
4. EXPERIMENTAL RESULTS AND DISCUSSION	20
4.1 PRELIMINARY STUDIES	20
4.1.1 SCREENING OF SILANE AND SILOXANE COMPOUNDS	20
4.1.2 THE EFFECT OF MORTAR AND EMULSION TYPE	20
4.1.3 THE EFFECT OF MORTAR ROUGHNESS AND EMULSION	22
4.1.4 CONTACT ANGLE TESTS FOR THE ICE ADHESION STUDY	23
4.1.5 ICE ADHESION: SPLITTING STRENGTH	24
4.2 THE EFFECT OF FIBERS	25
4.3 ICE ADHESION BY SHEAR TESTING	27
5. CONCLUSIONS	31

6. FUTURE WORK	31
7. REFERENCES	32
APPENDIX A: FALLING ROD IMPACT TEST AND PROCEDURE	35
APPENDIX B: FALLING ROD IMPACT TEST SAMPLE PREPARATION AND TEST	37
APPENDIX C: CONTACT ANGLES, ROLL OFF ANGLES AND MAXIMUM SHEAR STRENGTH RESULTS	38

LIST OF FIGURES

Figure 1: Number of US fatalities due to icy roads and risk zones (2009-2010 data) [1]	1
Figure 2: Invisible "black ice" on a bridge (left) and crash due to icy bridge (right) [1].....	2
Figure 3: Temperature for storm scenarios (top left), sample for shearing test (bottom left), and set up sketch for the shearing test (right) [5].....	3
Figure 4: Hydrophillic, hydrophobic, overhydrophobic, and superhydrophobic surfaces [9].....	4
Figure 5: The nature of chemical bond of silane/siloxane to concrete substrate [22].....	5
Figure 6: The chemical composition of siloxane based (polymethylmethoxysiloxane, left) and silane based molecules (trimethoxymethylsilane, right) [22, 24].....	5
Figure 7: SEM image of ZnO Nanotowers [31]	9
Figure 8: Schematic representation of coating procedure [38]	10
Figure 9: Sample beam in the centrifugal apparatus [40]	11
Figure 10: Schematic of the apparatus (a) PASCO stress/strain apparatus (b) Horizontal force applied to the ice column [15]	11
Figure 11: Laray falling rod viscometer	15
Figure 12: Silica fume SEM images (left) and X-Ray Diffractogram pattern (right).....	15
Figure 13: The procedure for preparation of emulsions.....	16
Figure 14: The set up for the specimen test (left), crushed specimens (center), and specimens treated with hydrophobic agent and bonded ice (right)	18
Figure 15: Setup of the splitting test.....	19
Figure 16: The specimen preparation for the ice adhesion tests (left and center) and the setup for the test (right)	20
Figure 17: The relationship between the ice loss and contact angle.....	21
Figure 18: The contact angles (left) and the roll-off angles (right) for tiles coated by different emulsions.....	22
Figure 19: Contact angles (left) and roll-off angles (right) for tiles with different roughness and volume of emulsion coating	23
Figure 20: The contact angle of coated tiles	23
Figure 21: Load vs extension for uncoated (left) and coated (right) W1 (w/c=0.7; s/c=5.5) specimens....	24
Figure 22: Load vs. extension for uncoated (left) and coated (right) W2 (w/c=0.5; s/c=2.75) specimens.	24
Figure 23: The ice fracture patterns of uncoated (left) and coated (right) specimens.....	25
Figure 24: The contact angle for tiles coated by E _{1S} and E _{1SR} emulsions.	26
Figure 25: Roll-off angles for tiles coated by E _{1S} and E _{1SR} emulsions.	26
Figure 26: The shear strength (ice adhesion) of specimens with fibers: a) M1, b) M2, c) M3, d) M4, and e) M5.....	28
Figure 27: The shear strength (ice adhesion) of plain specimens (without fibers): a) M6, b) M7, c) M8, d) M9, and e) M10.....	29
Figure 28: The correlation between the maximum shear strength and contact (left) or roll-off (right) angle	30
Figure A1: Ice loss on physical impact concept	35
Figure A2: Laray falling rod viscometer apparatus with timer.....	35
Figure A3: Ice adhesion via physical impact falling rod	36
Figure B1: Water Droplet dosed on tile.....	37

LIST OF TABLES

Table 1: Eutectic temperatures and concentrations [4]	3
Table 2: Chemical composition and physical properties of portland cement	12
Table 3: Mortar tile mix design.....	13
Table 4: List of siloxane/silane treatment materials	14
Table 5: Emulsion proportions.....	16
Table 6: The specimen mixture proportioning and icephobic treatment	18
Table 7: The effect of the agent on hydrophobicity and ice adhesion	21
Table 8: Splitting strength for coated and uncoated specimens.....	25
Table C1: Contact angles for tiles exposed to E1S and E1SR emulsions.....	38
Table C2: Roll off angles for tiles exposed to E _{1S} and E _{1SR} emulsions.....	38
Table C3: The correlation between the maximum shear strength and contact or roll-off angle.....	39

ANTI-ICING AND DE-ICING SUPERHYDROPHOBIC CONCRETE TO IMPROVE THE SAFETY ON CRITICAL ELEMENTS OF ROADWAY PAVEMENTS

EXECUTIVE SUMMARY

Fatalities due to icy road conditions average 467 per year in the U.S. The road ice hazard corresponding to these driving conditions results primarily from highway-speed travel during light winter precipitation events and has led to even more injuries and substantial property losses each year. The moderate and high risk zones primarily cover the Midwest and extend into Texas and Oklahoma, where high-speed travel is combined with both anticipated and unexpected road ice due to precipitation such as freezing rain, drizzle, fog (invisible ice) and snow. The majority of deaths and serious injuries occur during these conditions; however, the most accidents occur in critical areas, which include bridges, overpasses, elevated roadways, steep hills, curves, acceleration/deceleration spots, tunnels, and rural roads.

Strategies that have been used to diminish the road ice hazard involve the application of chemicals on roadways and the use of mechanical means to remove excessive snow accumulations. The National Cooperative Highway Research Program (NCHRP) publishes guidelines for the use of such materials along with methods for their application. There are other publications that recommend anti-icing practices and anti-icing chemicals, which are primarily salts that prevent or break the snow/ice bond to pavement through freezing point depression. These compounds have other well-known side effects, such as entry into groundwater and promotion of infrastructure corrosion and vehicle corrosion.

Anti-icing materials that form a physical or chemical bond to the pavement surface are desirable and this research included the evaluation of such materials from commercially available silanes and siloxanes. The overall objective was to select the appropriate treatment that would impart icephobic properties to concrete. Icephobicity has been extensively investigated for metallic, ceramic, and polymeric materials but has had little application in concrete. Treatments have consisted of a wide range of micro- and nano- icephobic coatings with different surface chemistries and topographies and they can be divided into four categories: low surface energy coatings, heterogeneous and composite coatings, superhydrophobic and porous materials, and use of other methods. It was demonstrated that hydrophobicity can be increased by exploiting surface roughness, particularly hierarchical roughness, where small particles lie atop larger particles in a hierarchical orientation. In this work, overhydrophobic and superhydrophobic silane and siloxane treatments were examined for icephobicity. Commonly, these materials are readily soluble in undesirable volatile organic compounds (VOCs); however, in this work, zero-VOC emulsions were produced and the use of silica fume particles (for inducing the roughness) was evaluated.

The first phase involved the evaluation of potential materials and development of test methods for icephobicity. Thirteen candidate silane and siloxane compounds were screened as potential superhydrophobic treatments on small plain mortar tiles (15mm x 15mm by 8mm thick), produced with a water to cement ratio (w/c) of 0.5 and sand to cement ratio (s/c) of 2.75. The treated tiles were tested for hydrophobicity via water droplet contact angle on their surface. The tiles and treatments were also evaluated for icephobicity using an ice loss on impact test that was developed as part of this project. This test utilized a falling rod striking a preformed and pre-weighed ice droplet on a tile and quantified the ice loss. Assessment of contact angle and ice loss enabled a narrowing of the material list to provide the candidates for water-based emulsions, along with one aqueous solution.

In addition to simple emulsions, the incorporation of silica fume particles was investigated. Here, silica fume was used to modify the emulsion using “shell” and “core” approaches. Core emulsions are where particulates reside inside the oil droplet phase, whereas for shell emulsions, the particulates reside in the continuous phase surrounding the droplets sometimes near the droplet interface. A procedure for production of emulsions was developed using polyvinyl alcohol (PVA) as an emulsifier. Treatments were evaluated on the 15 mm mortar tiles, with two different mortars (w/c=0.3 and 0.5; and s/c=1.0 and 2.75, respectively) and three treatment dosage levels (0.09, 0.18 and 0.35 l/m², respectively). Additional testing was performed to examine the effects of other dosages and varying roughness, imparted by the use of varying grits of silicon carbide paper. As a result of this work, by assessing contact angle and tilt-table droplet roll-off angle measurements, shell-type emulsions at nominally 10 µl dosage (0.045 l/m²) per tile were selected for further studies.

Separately, an ice-mortar splitting test for ice adhesion was developed. Here, half ice and half mortar 50-mm cubes were produced, with the ice half being cast onto both untreated and siloxane emulsion treated mortar half-cubes. Mortars with two different w/c and s/c ratios were used. The splitting force at the ice-mortar interface of the composite cubes was quantified using a splitting test. It was demonstrated that treatment helped to reduce the splitting strength, however, more significant was the effect of higher w/c and s/c ratios. This demonstrated that the aggregate proportions can play a large role in ice adhesion, sometimes dominating the effects of hydrophobic treatment, and indicating that w/c and s/c ratios should be included in future work.

Another icephobicity test was developed to quantify ice-mortar adhesion shear strength developed by an ice cylinder formed on a 15-mm square mortar tile. The ice cylinders were cast onto the tiles and removed under shear using a stress-strain apparatus. The test enabled the characterization of multiple mortar and treatment combinations affecting the ice adhesion.

Based on the aforementioned screening work, ten concrete mortar mix designs were prepared, five with fibers, five without, and with varying w/c and s/c ratios. Polymethyl-hydrogen-siloxane in a silica fume shell emulsion was selected and applied at two treatment concentrations, 5% and 25%. The treated tiles had significantly higher icephobicity, with the shear stress for ice removal

in the range of 0.02 to 0.12 MPa (3 to 17 psi) for treated tiles and 0.18 to 0.33 MPa (26 to 48 psi) for untreated specimens. On average, coated tiles had reduced ice adhesion by factors of 5 to 6 vs. their untreated counterparts. The top three performers had adhesion reduced by factors of 8.3 to 11.6, while reduction factors for the least effective three ranged from 2.6 to 3.

In an effort to achieve superhydrophobicity, concrete surfaces became icephobic, reducing the ice bond strength by factors on the order of 10+. This will allow for ice to be removed easily from the road surface. Since water is not allowed to penetrate concrete, freeze-thaw and corrosion resistance can be enhanced.

In addition to improved safety on the roads and facilitated freight mobility, the developed material can provide extended life spans for critical elements of bridges and other transportation infrastructure. Moreover, the use of icephobic materials in highway infrastructure can significantly reduce the need for maintenance and de-icing treatments.

1. INTRODUCTION

Adequate road conditions are vital for the performance of transportation infrastructure and safety. There are on average 467 fatalities per year due to icy road conditions in the U.S. [1]. Even more injuries and substantial property losses occur each year as a result of primary and/or secondary effects from loss of vehicle control on ice. Figure 1 shows the number of fatalities by state and the icy road risk zones based on the 2009-2010 data [1, 2]. The moderate and high risk zones primarily cover the Midwest and extend into Texas and Oklahoma.

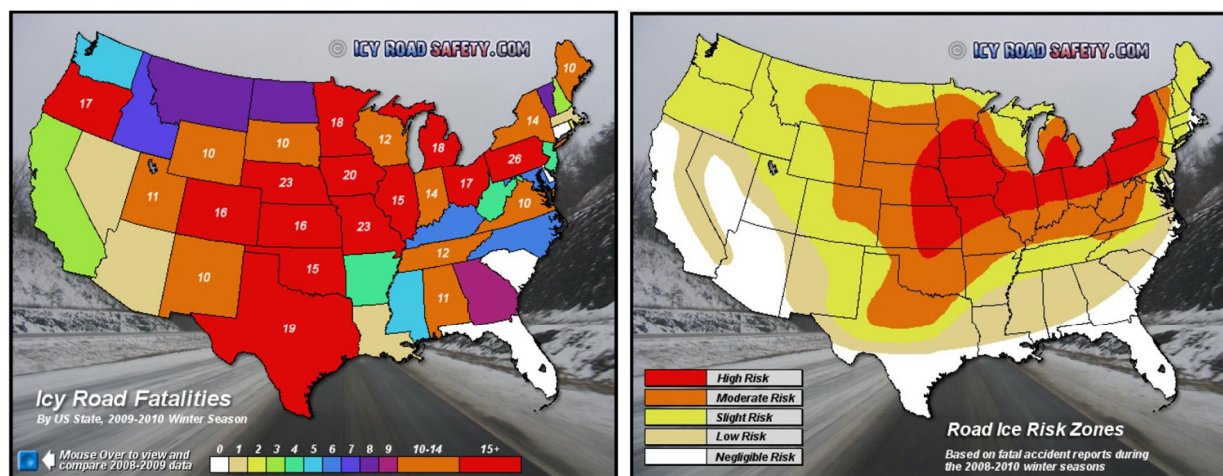


Figure 1: Number of US fatalities due to icy roads and risk zones (2009-2010 data) [1]

According to Dan Robinson the road ice hazard is defined by the conditions and situations where icing has the highest impact on life and property [1]. These factors are high-speed travel (above 45 mph, interstates, rural 2-lanes), the element of surprise (including bridges), subtle and intermittent icing (not visibly prominent), light winter precipitation (snow and freezing rain), and freezing rain, drizzle, and fog (invisible ice; Figure 2, left). In essence, the road ice hazard is primarily highway-speed travel during light winter precipitation events, when driver awareness is low and visual indicators are few.

The majority of deaths and serious injuries occur during these conditions; however, the most accidents occur in the following critical areas [1]:

- Bridges, overpasses and elevated roadways (Figure 2, right);
- Steep hills;
- High speed roadways;
- Curves;
- Deceleration spots;
- Acceleration spots;
- Low-traffic roads;
- Trouble spots include highway exit ramps, driveways, parking lots, and rural roads;
- Tunnels;
- Cobblestone and brick pavement.



Figure 2: Invisible "black ice" on a bridge (left) and crash due to icy bridge (right) [1]

In order to diminish the road ice hazard, different strategies have been used on roadways to remove snow and ice. The National Cooperative Highway Research Program (NCHRP) publishes the guidelines for materials and methods for their applications. The methods are classified as: a) anti-icing, b) deicing, c) mechanical removal of snow and ice together with friction enhancement, and d) mechanical removal [3]. These strategies involve the application of chemicals on roadways and the use of mechanical means to remove excessive snow accumulations.

Ketcham *et. al.* (1996), published recommendations for successful anti-icing practices for various combinations of precipitation, pavement temperature, traffic volumes, and mandated levels of service [4]. The guidance is based upon the results of 4 years of anti-icing field testing conducted by 15 State highway agencies and supported by the Strategic Highway Research Program (SHRP) and the Federal Highway Administration (FHWA). Recommended anti-icing practices were made for different anti-icing treatments based on the following chemicals: sodium chloride (NaCl), magnesium chloride (MgCl₂), calcium chloride (CaCl₂), calcium magnesium acetate (CMA), and potassium acetate (KAc).

Eli Cuelho *et. al.* (2010), reported on commonly available anti-icing chemicals applied on concrete and asphalt pavements at four application rates and under three temperature scenarios [5]. Sodium chloride, magnesium chloride, calcium chloride, potassium acetate, and a chemical made from agricultural by-products were tested. Results demonstrated that the use of anti-icing chemicals reduced the bond strength and the temperature at which the bond between the snow and the pavement failed. Field tests demonstrated improvements in performance for most chemicals through the reduction or elimination of the snow-pavement bond. It was concluded that effective anti-icing chemicals can provide safe driving conditions during winter maintenance, reducing costs as well as impacts on the environment and infrastructure.

Storm Scenarios	Initial Conditions		
	Pavement Temperature °F (°C)	Snow Temperature °F (°C)	Air Temperature °F (°C)
I (P14-SA14)*	14 (-10)	14 (-10)	14 (-10)
II (P32-SA23)*	32 (0)	23 (-5)	23 (-5)
III (P32-SA30)*	32 (0)	30 (-1)	30 (-1)

*P = Pavement temperature and SA = snow and air temperature in degrees Fahrenheit

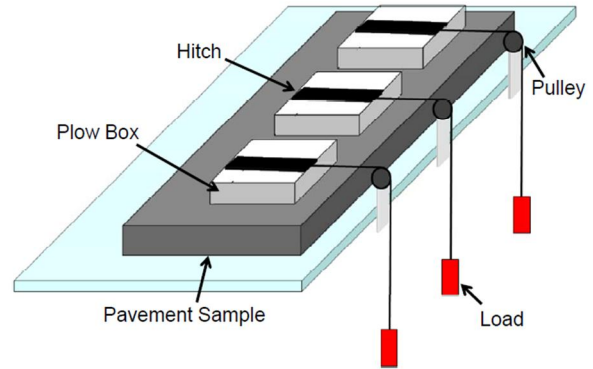


Figure 3: Temperature for storm scenarios (top left), sample for shearing test (bottom left), and set up sketch for the shearing test (right) [5]

Most of these strategies rely on chemicals which act as a coat on the pavement surface (anti-icing) to prevent or to break the bond between snow or ice and the pavement surface (deicing). Ketcham *et. al.* (1996), present a table used to recommend the eutectic temperatures and concentrations of applicability of different anti-icing materials [4]. Due to temperature changes, traffic load, and pavement maintenance operations, these chemicals dissolve and disperse into the nature. Wisconsin Transportation Bulletin reported some cases where ground waters with deicing chemicals were found in wells used as drinking water sources [6]. These chemicals may cause deterioration in concrete and steel structures, as well as accelerate vehicle corrosion. Despite all these disadvantages, chemicals used to reduce the road ice hazard are in widespread use.

Table 1: Eutectic temperatures and concentrations [4]

Chemical	Eutectic temperature °C (°F)	Eutectic concentration %
calcium chloride (CaCl ₂)	-51 (-60)	29.8
sodium chloride (NaCl)	-21 (-5.8)	23.3
magnesium chloride (MgCl ₂)	-33 (-28)	21.6
calcium magnesium acetate (CMA)	-27.5 (-17.5)	32.5
potassium acetate (KAc)	-60 (-76)	49

Anti-icing materials with a physical or chemical bond to the pavement surface are more desirable than materials currently in use. Chemically attached anti-icing materials can have a higher durability at relatively small amounts of material use. With beneficial characteristics such as enhanced performance and reductions in chemical use, personnel, and equipment, there is a need for new materials which reduce ice adhesion to the pavement surface in a sustainable and environmentally friendly manner. In this respect, hydrophobic and superhydrophobic coatings are promising.

1.1 HYDROPHOBICITY AND SUPERHYDROPHOBICITY

The hydrophobicity of a material is defined as the ability of the material to repel water and depends on the surface chemical composition and the surface geometry (micro- and nano-structural morphology) [7]. The contact angle between a drop of water and the surface is generally used as an indicator of hydrophobicity or wettability. When the contact angle is greater than 90° , it indicates hydrophobicity, while a contact angle less than 90° denotes hydrophilicity, which is the tendency of a surface to become wet or to absorb water, as shown in Figure 4. Common concrete is an example of a hydrophilic mesoporous material which absorbs water. The superhydrophobicity corresponds to contact angle between 150° and Surfaces with intermediate properties, with high contact angles between 120° and 150° , above typical values for hydrophobic materials, are called “overhydrophobic.” The water contact angle with a solid surface can be measured by goniometer or tensiometer [8].

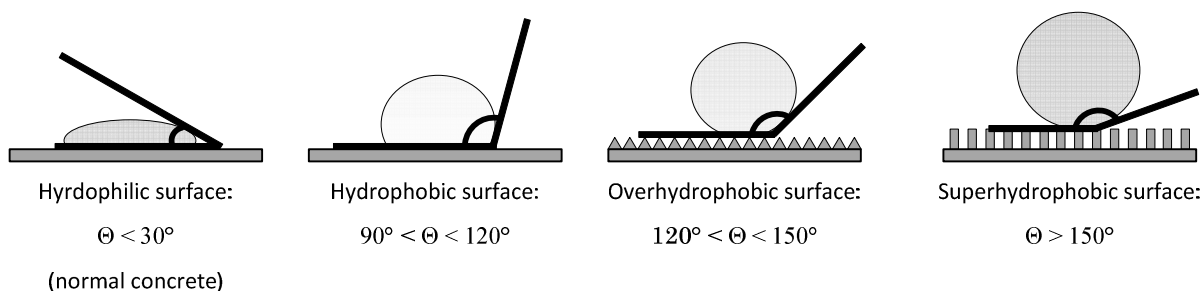


Figure 4: Hydrophilic, hydrophobic, overhydrophobic, and superhydrophobic surfaces [9]

Superhydrophobic hierarchical surfaces with hierarchical roughness patterns imposed over larger roughness patterns have generated interest due to their potential in industrial applications (mainly, for self-cleaning). These surfaces mimic the Lotus leaf surface, which is well known for its superhydrophobicity and self-cleaning properties, (Lotus-effect). Mimicking living nature for engineering applications is called “biomimetics,” and biomimetic approaches can be used to synthesize hydrophobic and superhydrophobic concrete [10-15].

1.2 HYDROPHOBIC COATINGS ON CONCRETE BASED MATERIALS

Waterproofing and the incorporation of hydrophobic additives into the concrete matrix are two approaches used to improve the physical properties of concrete. The first approach consists of using hydrophobic materials on the surface of concrete to repel water [16], which also improves the freeze thaw durability of concrete. The type of material and quantity used affects its concrete protecting efficiency [17]. The second approach consists on creating a hydrophobic concrete or cement matrix using admixtures [11, 18-20]. The addition of an admixture of a hydrophobic nature into the concrete mix represents a viable possibility to achieve a good quality concrete.

1.2.1 WATERPROOFING TREATMENTS.

Many admixture companies (e.g., Wacker, Kryton, Xypex) offer ready to use products for the surface waterproofing or sealing of concrete as a protection against corrosion on reinforcing steel, chemical corrosion, cracking, frost damage, salt damage, lime leaching, fungal, moss, and stains, etc. [21]. Most of these products, and those found in the literature, are based on silanes

and siloxanes, along with some variations, such as sodium silicate, silicone resin solution, silane/siloxane, silane/siloxane with an acrylic topcoat, alky-alkoxy silane, two component acrylics, silicone in turpentine, siloxane acrylic, thixotropic cream (based on octyltriethoxy silane), water based solution of alkylalkoxysilane, and acrylic latex.

In contrast to other hydrophobic materials, silanes and siloxanes have smaller molecular sizes than epoxies and acrylic agents, which allow these compounds to reach smaller pores resulting in more effective surface treatments. In addition to the smaller size, the alkoxy groups can chemically bond to the hydrated silicates, while the hydrophobic alkyl groups essentially protrude from the surface, as depicted in Figure 5 [22]. Silanes differ from siloxanes in the chain length (Figure 6). The former are small molecules with one silicon atom, while the latter are larger molecules with several silicon atoms. In addition to their hydrophobic effect, these substances reduce the bond between the ice and concrete [23].

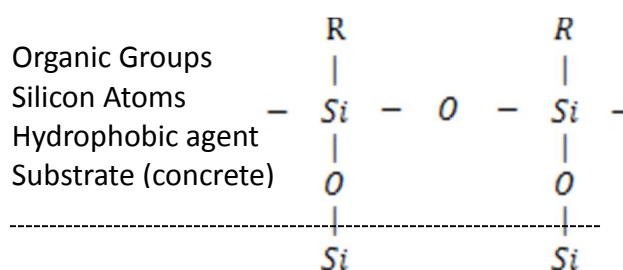


Figure 5: The nature of chemical bond of silane/siloxane to concrete substrate [22]

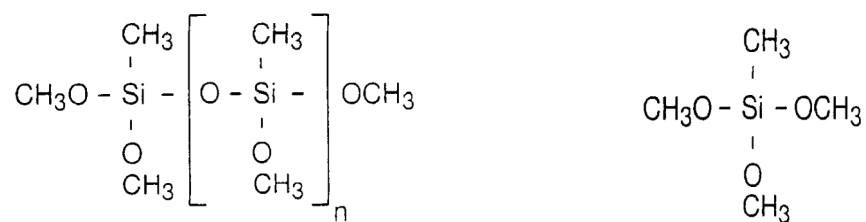


Figure 6: The chemical composition of siloxane based (polymethylmethoxysiloxane, left) and silane based molecules (trimethoxymethylsilane, right) [22, 24]

The efficiency of these materials depends on their penetration depths into concrete, their resistance to adverse environmental factors, and the ability of their chemical composition to limit the penetration of damaging species, such as chloride ions and carbon dioxide, into the material. Basheer et al., (1997) reviewed and summarized some methods used to evaluate water and ion penetration in concrete, and included the evaluation of the surface treatments in general [25]. The tests for evaluating the transport processes in treated substrate were classified into water vapor permeability (breathability) and water absorption.

Basheer et al. (1997) presents a comprehensive list of the methods used to assess the efficiency of different surface treatments and categorizes them into water penetration resistance tests and water absorption tests [25]. The resistance offered by the hydrophobic surface to water penetration can be measured by exposing the treated surface to water after sealing the other

surfaces, or by submerging the entire sample in water, and measuring the change in weight of the samples over a specific amount of time. The National Cooperative Highway Research Program (NCHRP) report 244, recommends that, to be accepted, any surface treatment should reduce water intake at least by 75% compared to untreated surfaces [26]. However, highly porous materials, such as concrete and masonry, were not considered in this report. The German Committee for Reinforced Concrete considered porous materials and recommended a limit for water absorption of 2.5% by mass and a reduction of 50% compared to untreated surfaces [27].

The most effective coating chemicals were found to be some epoxies, along with silane and siloxane based materials. Basher et al., (1997) also reported the effectiveness of a second coat and the use of undiluted silane materials [25]. Xiaojian (2011) reported on the effect of silane surface treatment on water adsorption [23]. Silane treated specimens absorbed water quicker in the first hour, but over time the percent of water adsorption tended to a stable value, while in non-treated concrete this value continuously increased. Air-entrained samples demonstrated higher water adsorption than non-air-entrained. Also reported was that high strength concrete and surface treated concrete withstood freeze and thaw cycling better than their lower strength and untreated counterparts.

An important and practical aspect of hydrophobic surfaces was reported by Ibrahim and Al-Gahtani (1999), relating to the effects of surface treatments on the degradation of reinforcing steel when exposed to detrimental conditions [28]. The effects of chloride-induced corrosion and carbonation and sulfate attack were studied by measuring the reduction in compressive strength of concrete specimens ($w/c = 0.45$) protected by 6 different surface treatments: sodium silicate, silicon resin solution, silane/siloxane, silane/siloxane with an acrylic topcoat, alkylalkoxy silane and a two component acrylic coating. These sealers were not able to prevent the sulfate attack, carbonation or chloride ingress. However, they did reduce the chlorides concentration in specimens exposed to chloride solutions for 3 months, and reduce the carbonation depths after 5 weeks of exposure compared to uncoated or untreated concrete. After 330 days of immersion in sulfate solution, the specimens had a lower reduction in compressive strength than uncoated specimens. The most effective chemicals were the combinations of silane and siloxane with an acrylic topcoat.

The fact that hydrophobic treatments do not completely protect concrete may be explained by the work of Tittarelli, et al., (2000) related to oxygen diffusion through hydrophobic matrices [29]. The oxygen reduction current under at a steady potential was measured on samples of a steel plate reinforced concrete with a w/c ratio of 0.45 and 0.8 and coated with a siloxane based commercial product. . The current level was proportional to the presence of oxygen in the matrix. After casting, all the specimens demonstrated high content of oxygen which probably lodged in the air voids. However, when non-hydrophobic specimens were immersed in water, the current dropped as a result of the decrease of oxygen diffusion into the matrix. The presence of water in the voids blocked the diffusion of oxygen into the concrete. In contrast, for hydrophobic concrete, the lack of water in the voids allowed a continuous supply of oxygen. This research also reported the correlation between the tests on mortars and concrete. At the same w/c , the diffusion of oxygen is higher in concrete than in mortars, probably due to the porous interfacial zone between the aggregate and cement paste.

1.2.2 HYDROPHOBIC ADMIXTURE TREATMENTS

Hydrophobic admixtures added during cement milling have been used to preserve the powdered cement from humidity in the environment. The addition of these chemicals to stored cement prevents early hydration. However, the hydrophobic protection fades during the concrete mixing process (Popovics, 1982); consequently, this type of hydrophobic admixtures is not designed to protect concrete from freezing and thawing [18].

The type of hydrophobic admixtures that may affect the freeze-thaw resistance of concrete would have to be incorporated into the fresh mix. The chemicals reported to add hydrophobicity to the bulk of concrete were mineral oil, vegetable oil, paraffin waxes, calcium stearate, hydroxynaphthenic acids, sucrose mono-palmitate, sucrose distearate, zinc stearate, silicon sucrose trioleate, hydrocarbon resins and bitumen [19, 20], aqueous emulsions of alkyl-triethoxy silane [30], and an aqueous emulsion of butyl-ethoxy-silane [29]. The complete classification of silico-organic compounds used for concrete hydrophobization was proposed by Batrakov, (1990) [24]. Most of these chemicals have some negative effects on concrete mix, e.g., oleates affect the monosulfate reaction, stearates decrease the setting time of cement pastes, acids may alter the pH of concrete, and almost all were reported to lower the compressive strength of concrete or mortars. Only samples containing corn oil at relatively low dosages, 0.25% by weight of cement added to mortar as an emulsion, demonstrated higher values of compressive strength than the control samples [19]. Tests performed on mortars of with a water-to-cement ratio of 0.3 and incorporating corn oil and stearic acids at different dosages, indicate that these hydrophobic admixtures act as retardants and also act as densifying materials by reducing porosity (initial and long-term). These samples were also tested for water absorption at different curing ages and over a soaking period. All mortars with hydrophobic agents yielded reduced water absorption compared to reference samples [19, 20].

Tittarelli et al. (2000) reported on the effects of hydrophobic concrete on the corrosion of steel in the presence or absence of cracks in concrete [29]. Specimens with water-to-cement ratios of 0.45 and 0.8 were immersed in a sodium chloride solution, and tested for electrochemical potentials, visual observations and weight loss. It was concluded that the use of silane blocks the corrosion process in uncracked concrete, but worsens the damage in cracked concrete.

Sobolev and Batrakov (2007) reported that concrete's resistance to freezing and thawing was improved by the application of siloxane-based emulsion used as an admixture [11]. The high reactivity of the siloxane (polyethyl hydrogen siloxane, PEHSO) is due to the large number of (-Si-H) sites that react with the hydroxyl groups of cement (or portlandite) resulting in the generation of hydrogen, and formation of a stable hydrophobic pore structure. The use of the emulsion at 0.065% in the concrete mix creates up to 2-3% of hydrogen formed within the volume (while air-entraining agents are commonly used at 0.1-0.5% to create 5% of air voids, according to specifications). The size of the pores within the paste can be manipulated by varying the droplet size of the siloxane in the emulsion. Optimal performance in concrete can be achieved when more than 70% of the droplets are less than 1 micron. The emulsion used contained 50% siloxane and a polyvinyl alcohol emulsifying agent. It was mentioned that the hydrogen released caused a slight expansion of the concrete during the first hours of hydration due to internal pressures of up to 0.05 MPa.

2. DEVELOPING THE ICEPHOBIC PROPERTIES

Icephobicity investigations have been extensive for metallic, ceramic, and polymeric materials but have been limited with respect to concrete [15]. For these materials icephobic coatings are commonly used to help prevent ice formation. It has been proven in many cases that superhydrophobic coatings have a limited ability to prevent ice formation on metallic surfaces thus leading to an interest in icephobicity properties as affected by chemical composition, methodology and testing.

2.1 CHEMICAL COMPOSITION

Coatings and solutions consisting of a wide range of micro/nano icephobic materials with different surface chemistries and topographies have been tested for icephobicity. They can be divided into four categories; low surface energy coatings, heterogeneous and composite coatings, superhydrophobic and porous materials, and use of other methods [31].

Low surface energy coatings can use poly (dimethyl-siloxane) (PDMS or silicone), Teflon[®] (polytetrafluoroethylene, PTFE). In their review, Menini *et al.* (2011) summarized that the relatively low adhesion between ice and polysiloxane-based polymers is due to their dissimilar rheological-mechanical properties; with the polymers having low T_g values, they tend to be flexible or lubricating at the interface [31]. Mulherein and Haehnel (2003) tested 16 different commercial materials claiming to be ‘icephobic’ and concluded that these products were successful in reducing the amount of energy to remove ice, but had limited ability to prevent the build-up of ice [32]. Sarshar *et al.* (2012) demonstrated that nano-structured superhydrophobic powder can be produced by bonding a low surface energy coating (tridecafluoro-tetrahydroctyltrichlorosilane) to commercially available powdered silica nanoparticles (99.9 % SiO₂, 10–100 nm particle size) using a fluorination procedure. The silica nanoparticle powder was mixed with a commercial product polyurethane clear coat using an ethanol acetone solvent mixture [33].

The formation of heterogeneous chemistries on a surface using two or more hydrophobic agents, disrupts the water film (“liquid like layer”) at the ice-surface interface, reducing ice adhesion [31]. Heterogeneous and composite coatings that are a mix of polysiloxane and fluorocarbon materials can lower ice adhesion better than homogeneous coatings with either PDMS or the polyfluorocarbon (PFC) type of structures. Farhadi *et al.* (2011), Kulinich *et al.* (2010) and He *et al.* (2010) tested coatings of organosilane, fluoropolymer and silicone rubber on rough surfaced aluminum [34-36]. Results demonstrate that the aluminum surfaces coated with hydrophobic room temperature vulcanized silicone rubber resists ice formation. They showed the coating can largely prevent ice formation on the surface, except for a few ice growth spots at a working temperature of -6 °C. However, the coating was covered by a layer of ice after 30 min of spraying super cooled water [34-36].

Superhydrophobic or porous coatings reduce the surface area of a material thus leading to less bond and stress concentrations. Surface roughness can have a significant influence on hydrophobicity. In this way a liquid-infiltrated porous solid retains liquid on the material exhibiting low contact angle hysteresis. Menini *et al.* (2011) reviewed multiple methods used to enhance surface roughness and porous structure, such as etching a substrate, depositing nanoparticles, utilizing nanolithography, and electroplating polymers or ZnO ‘nano-towers’ as

shown in Figure 7 [31]. The addition of a low surface energy thin film has been used employing various techniques such as plasma enhanced chemical vapor deposition (PECVD), deposition of self-assembled monolayers (SAM) and passivation with stearic acid. This allows the frozen droplets to slide off with minimal force and has many characteristics for icephobicity in aluminum [31].

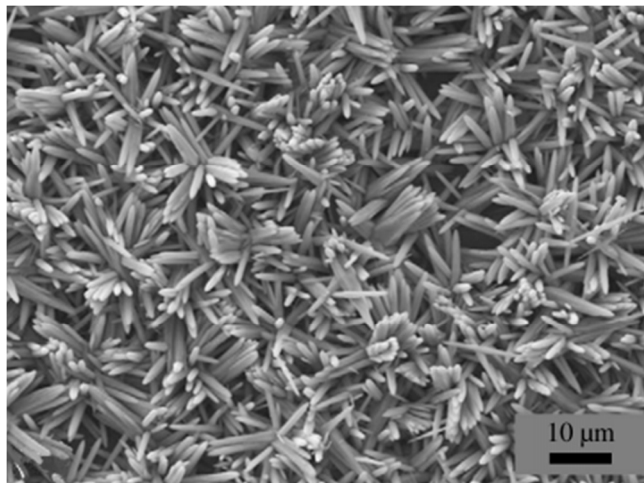


Figure 7: SEM image of ZnO Nanotowers [31]

Other methods were described by Guo *et al.* (2012) who tested a micro/nanostructured surface (MN-surface) composed of micro scratches combined with nano-hairs on a metal substrate. It was found that the MN-surface has a robust icephobic property relative to that of nanostructured and micro-structured surfaces and smooth surfaces without any structure [37].

2.2 APPLICATION METHODS

Some common methods of application include spinning, dipping, spraying, or combinations of these. The thickness of the coating during the application process must be monitored for consistency. In many instances before a coating is applied the roughness of the material needs to be determined.

Kulinich and Farzaneh (2009) used multiple coating methods [38]. A summary of the coating process is given in Figure 8. Before coating the material the samples were polished with emery paper and cleaned in organic solvents. Centrifugated particles (7.0 g) were mixed with 80 ml of deionized water. Suspensions were sonicated for 30 minutes, and then 6.0 ml Zonal 8740, a perfluoroalkyl methacrylic copolymer product was added and mixed for 3 hours. The first group of samples was sprayed 10 cm from the surface until the surface was fully covered. The second group of samples was spin-coated at a spinning speed of 200 rpm for 5 seconds and 3000 rpm for 10 seconds. These samples were compared with a without nanoparticles. After coating these samples were heat treated at 120°C in air for 3 h to remove the residual solvents [38].

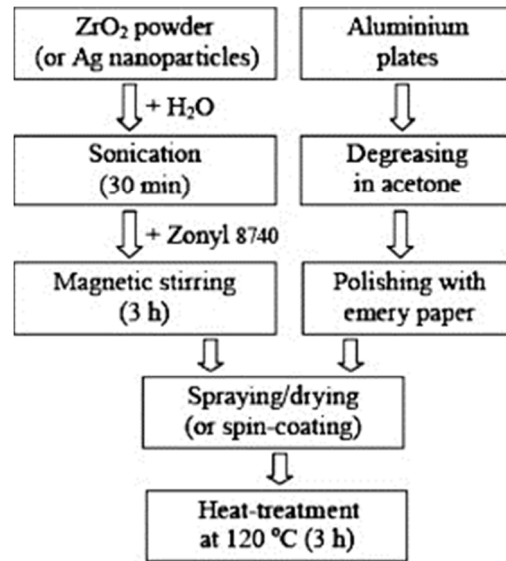


Figure 8: Schematic representation of coating procedure [38]

Cao *et al.* (2009) prepared a sample of coated aluminum by first mixing 2.5 g of the organosilane-modified silica particles of various diameters (20 nm, 50 nm, 100 nm, 1 μ m, 10 μ m, and 20 μ m) with 5 g of the polymer binder, 75 g of toluene, and 15 g of acetone. They applied the particle – polymer composite by using a spray gun at a pressure of 20 psi and then cured the coating at a room temperature for 12 hours [39].

Sarshar *et al.* (2012) tested icephobicity using aluminum samples with icephobic coatings. To create a rough surface the sample was lightly sanded with 900 grit wet-and-dry sandpaper using acetone and isopropyl alcohol. The coating was spray deposited with varying thicknesses of 15–20 μ m and 25–30 μ m [33].

2.3 TESTING PROCEDURES

There are multiple techniques and apparatuses used to test ice adhesion. The most common methods utilize wind tunnels as well as centrifugal force and shear force devices. Each test is used to determine the performance of an icephobic coating by calculating the force to remove the ice from the material.

Kulinich *et al.* (2010) performed tests by spraying super cooled micro droplets of water in a wind tunnel at subzero temperature to simulate freezing rain [35]. Samples were iced in a wind tunnel and sprayed with super cooled micro droplets with an average size of 80 μ m. They were then spun in a centrifuge apparatus at constantly increasing speed. A Peltier device supplied with the goniometer used kept the droplets frozen and condensed from the ambient air. The contact angle and contact angle hysteresis were measured by standard procedures [4]. The centrifuge apparatus also evaluated the adhesion and shear stress of ice detachment. Laforte *et al.* (2005) performed a test using centrifugal force to detach the ice layer (Figure 9) [40]. The ice detaches as the centrifugal force just overcomes the adhesion of the ice. When detachment occurs, two piezoelectric cells fixed to the sides of the apparatus relay the time to a computer and the rotation speed is determined. Depending on the coating, the test runs from 2 -20 seconds and is repeated for accuracy [40].

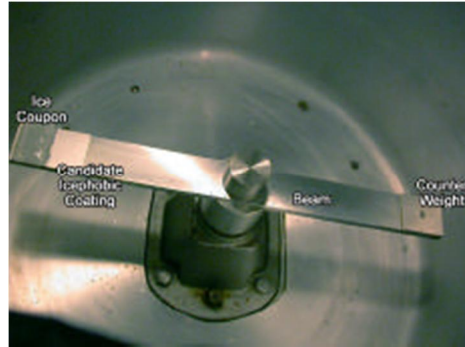


Figure 9: Sample beam in the centrifugal apparatus [40]

Zou *et al.* (2011) built a custom apparatus to test for ice adhesion by measuring the shear stress at which ice detaches from a specimen [41]. A 4 μL water droplet with a radius of 0.985 mm is placed on the surface to be tested. The conical tip is then aligned with the water droplet and lowered down to the sample surface until the contact force is zero. The conical tip and water droplet are then cooled to $\leq -10^\circ\text{C}$. During the test, the temperature and time are recorded and monitored. The apparatus is then nitrogen purged in an isolation box to avoid condensation. Digital images are taken during the test to determine the contact of the water droplet to the specimen. Once the droplet is completely frozen, the conical tip applies force on the water droplet, advancing at a rate of 1 mm/s. As the droplet has become detached, the two horizontal load cells record the average force to shear the frozen droplet. The shear stress can be calculated using the surface area from the digital images and the shear force to detach the frozen droplet [41].

Hejazi *et al.* (2013) used a PASCO CI-6746 stress-strain apparatus to test for the adhesion strength of ice by applying horizontal shear force until an ice column was separated from its substrate [15]. The testing equipment can be seen in Figure 10. Before testing, thin plastic tubes were placed vertically on the substrate surface and filled with water and kept in a freezing room at -20°C until the water was entirely frozen. It was then demolded and transferred to another freezing room with the temperature of $-3 \pm 2^\circ\text{C}$ where the stress-strain apparatus was used. The horizontal shear force was applied to the base of the ice column until it separated from the material. Measurements were recorded using DataStudio software [15].

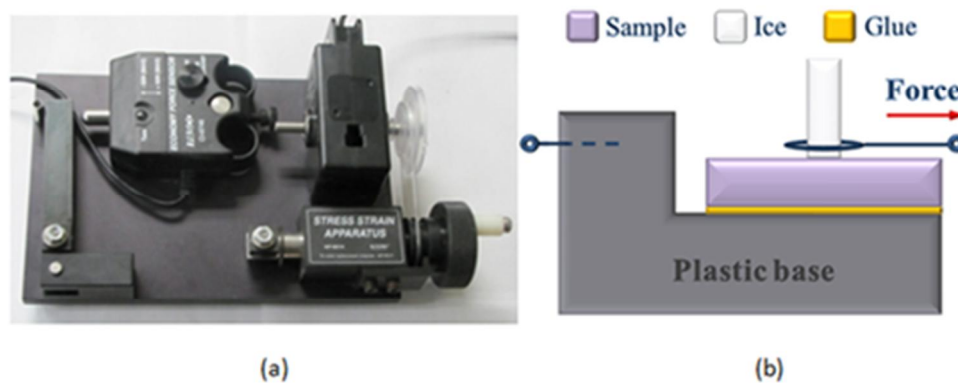


Figure 10: Schematic of the apparatus (a) PASCO stress/strain apparatus (b) Horizontal force applied to the ice column [15]

3. RESEARCH OBJECTIVES

A "smart" anti-icing and de-icing superhydrophobic concrete is proposed to prevent the formation of ice on roadway pavements and bridges. This method involves engineering the hierarchical concrete surface and the application of fibers with superhydrophobic siloxane admixture. The objectives of this research project are to: 1) introduce and develop an effective anti-icing and de-icing superhydrophobic concrete; and 2) assess the general feasibility of such a system through laboratory testing. The proposed superhydrophobic modification is based on a optimization of high-strength fibers (e.g., PVA), and aggregates as well as the use of siloxane-based hydrophobic emulsions with small quantities of super-fine, submicro or nanosized materials such as nanosilica or SiO₂-rich reactive powders. This composition, when used on concrete surfaces can provide superhydrophobic hybridization of concrete with anti-icing and de-icing properties.

3.1 MATERIALS AND EXPERIMENTAL PROCEDURES

3.1.1 MORTAR MATERIALS

Mortar specimens were prepared using a commercial Type I portland cement (PC) from Lafarge. The chemical composition and physical properties of cement are presented in

Table 2, along with the requirements of ASTM Standard Specification for Portland Cement (ASTM C150) [42]. ASTM C778-graded standard quartz sand [43] with an average particle size of 425 μm and tap water were used to produce mortar tiles and cubes. Polyvinyl alcohol (PVA) fibers (RECS 15x12 mm Kuralon K-II) with a diameter of 15 dtex (0.04 mm) and length of 12 mm were used in this study. These fibers had a Young's modulus of 40 GPa and a tensile strength of 1.6 GPa. The high-range water-reducing admixture used in the study was commercially available polycarboxylate ether superplasticizer (PCE/SP) with a 31% solid concentration.

Table 2: Chemical composition and physical properties of portland cement

CHEMICAL			PHYSICAL		
Item	ASTMC150 Limit	Test Result	Item	ASTMC150 Limit	Test Result
SiO ₂ , %	-----	19.8	Density, g/cm ³	-----	3.20
Al ₂ O ₃ , %	-----	4.9	Time of setting, minutes		
Fe ₂ O ₃ , %	-----	2.8	Initial	45 min	165
CaO, %	-----	63.2	Final	375 max	257
MgO, %	6.0 max	2.3	Compressive strength, MPa		
SO ₃ , %	3.0 max	2.9	1 day	-----	12.1
Ignition loss, %	3.0 max	2.8	3 days	12.0 MPa	21.7
Na ₂ O, %	-----	0.2	7 days	19.0 MPa	28.3
K ₂ O, %	-----	0.5	28 days	28.0 MPa	36.5
CO ₂ , %	-----	1.3			
Potential, %					
C ₃ S	-----	54.7			
C ₂ S	-----	15.5			
C ₃ A	-----	8.4			
C ₄ AF	-----	8.4			

$C_4AF+2(C_3A)$	-----	25.1
$C_3S+4.75(C_3A)$	-----	94.5
Na_2O_{equi}	0.6 max	0.57

3.1.2 PROPORTIONS OF PORTLAND CEMENT MORTARS

For mortars used, the water to cementitious material (W/C) ratio, sand to cementitious material (S/C) ratio, superplasticizer dosage (by weight of cement, solid content), and PVA fiber (volume content) are shown in Table 3. Preliminary work was performed on mortars A, B and C, where no fibers were used. PVA fibers were used in M1-M5 series, where the dosage of the fibers was 1%. Superplasticizer dosage was adjusted to achieve a workable mortar (Table 3).

Table 3: Mortar tile mix design

MIXTURE ID	PRELIMINARY			WITH FIBERS					WITHOUT FIBERS				
	A	B	C	M1	M2	M3	M4	M5	M6	M7	M8	M9	M10
W/C	0.7	0.5	0.3	0.25	0.3	0.4	0.45	0.5	0.25	0.3	0.4	0.45	0.5
S/C	5.5	2.75	1.0	0	1	2	2.5	3	0	1	2	2.5	3
SP, % solid	0	0	0.1	0.14	0.1	0.1	0.1	0.1	0.42	0.045	0.04	0.02	0.01
PVA Fibers, % vol	0	0	0	1	1	1	1	1	0	0	0	0	0

3.1.3 TYPE AND PREPARATION OF SPECIMENS

Relevant ASTM standards were used for mixing (ASTM C 305) [44], casting, demolding and storage (ASTM C 109) [45] of mortar specimens. Cubes and tiles with dimensions of 50x50x50 mm and 15x15x8 mm were prepared, respectively. Specimens were allowed to harden for 24 hours at 23±3 °C and at least 90% of relative humidity. Specimens were demolded 24 hours after the mixing procedure, and they were allowed to cure in lime saturated water for 72 hours.

3.1.4 PRELIMINARY STUDY – SCREENING OF SILANE AND SILOXANE COMPOUNDS

The commercially available products evaluated were selected in order to encompass a variety of modified silane and siloxane chemical functionalities. Table 4 lists the materials examined. 25% active ingredient solutions were produced for all treatment materials, with most being dissolved in isopropyl alcohol and sodium methyl silicate and potassium methyl silicate salts being dissolved in water. Emulsions were not used, since this experiment was used for screening the selected materials for effectiveness. All mixes were made by gravimetrically adding active compound to its solvent in a HDPE bottle and manually shaking for approximately 1 minute.

Tile specimens produced from mortar mix “B” were used in this investigation. All tiles were dry sanded using 40 grit belt sanding in two steps: the first to flatten the tile surface and the second to sand the flat surface. Each step was performed as follows: with the sander on and the belt in motion, the tile was pressed against the belt with a force of approximately 5 lb and moved back and forth perpendicular to the belt direction 5 times for approximately 3 seconds; the tile was rotated 90 degrees and the process repeated. The tile was visually examined after each sanding to confirm that material removal was uniform and the surface was visually flat. After sanding, tiles were rinsed in tap water, ultrasonically cleaned in tap water for 5 min, again rinsed in tap water, again ultrasonically cleaned in tap water for 5 min, rinsed in distilled water, dried at 110 °C for 3 hours, and allowed to cool at room temperature for 24 hours. Each tile was individually soaked in a single solution for 30 minutes. When removed, excess solution was manually shaken off and

the tile set on a flat surface. All tiles were allowed to dry at ambient room conditions for a minimum of 24 hours before contact angle measurements were made. Two tile repetitions were produced for each treatment.

Table 4: List of siloxane/silane treatment materials

Tile ID	Siloxane/silane active treatment	Applied of active material applied	Solvent
A00	Untreated/Reference	-	-
A01	Polymethylhydrogensiloxane	25%	isopropanol
A02	Polydimethylsiloxane, 200 cSt	25%	isopropanol
A03	Polydimethylsiloxane, 300 cSt	25%	isopropanol
A04	t-Butyltrimethoxysilane	25%	isopropanol
A05	N-(3-(Trimethoxysilyl)propyl)ethylenediamine *	25%	isopropanol
A06	Methyltrimethoxysilane	25%	isopropanol
A07	Hexamethyldisilazane	25%	isopropanol
A08	Phenyltrimethoxysilane	25%	isopropanol
A09	Aminosilsesquioxanes. methoxy-terminated *	25%	isopropanol
A10	Vinyltrimethoxysilane	25%	isopropanol
A11	n-Octyltriethoxysilane	25%	isopropanol
A12	Tetraethoxysilane	25%	isopropanol
A13	Sodium methyl siliconate	25%	water
A14	Potassium methyl siliconate	25%	water

* Primary component in alkoxy silane blend

A Kruss DSA100 “Drop Shape Analysis System” goniometer was used for sessile drop contact angle measurements. Deionized water was used as the liquid phase: 20 microliters of water was dosed onto the tile surface at 800 microliters/min from a distance of 2 mm above the tile surface using the instrument’s automatic syringe. The drop was allowed to stabilize for 22 seconds and the contact angle from the drop image was measured using the Kruss DSA4 Drop Shape Analysis software. Each of the tile repetitions was tested and the average value reported.

The impact test used in this preliminary study was the falling rod impact test procedure. The apparatus used for falling rod impact was a Laray falling rod viscometer, shown in Figure 11. In this test, a rod falls onto tile with a preformed (nominally) 0.13-0.14 g ice droplet. The rod strikes the ice droplet and the amount of ice lost is determined via weight change. Mortar tile specimens were chilled to -10°C (vs. -20°C used in later research) for 1 hour and 150 microliters of icy distilled water (vs. +10°C in final method) was placed on the tiles in the freezer. These specimens were chilled for another 30 min then impact testing performed at ambient room conditions (vs. +10°C used in later research). The tiles were pulled individually from the freezer for impact testing and the falling rod was placed in ice water for approximately 1 min between the tests and dried before the impact. One tile representing each coating was tested for ice loss (i.e., one “repetition” was tested for ice loss).

3.1.5 EMULSION MATERIALS

For emulsion stabilization, water soluble polyvinyl alcohol (PVA) was selected because of its nonionic character and perfect compatibility with concrete materials [46]. A highly hydrolyzed (98%) PVA with molecular weight of 16,000 from Acros Organics was used to reduce the

tendency of foam formation. Deionized water (DI water) was used as the dispersion medium for the emulsions. Polymethyl-hydrogen siloxane oil, PMHS (Xiameter[®] MHX-1107) from Dow Corning with a specific gravity of 0.997 (at 25°C) and a viscosity of 30 cSt was used as the hydrophobic agent. This product contains 85-100% of polymethylhydrogen siloxane as an active ingredient. Silica fume (SF) from Elkem was used in this research. The SF was analyzed by the X-ray powder diffraction (XRD) and scanning electron microscope (SEM) techniques. An X-ray diffractogram and microscope image (Figure 12) reveals an amorphous structure of spherical silica particles.



Figure 11: Laray falling rod viscometer

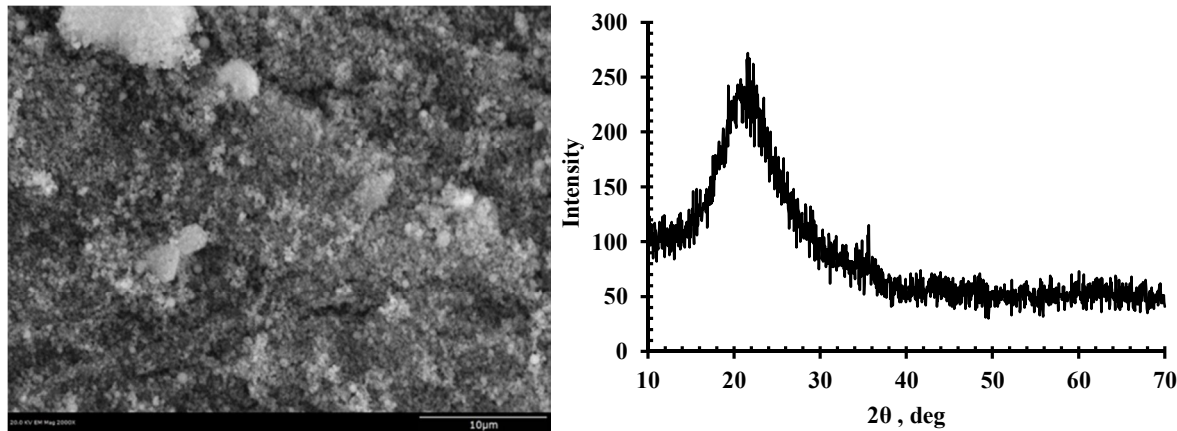


Figure 12: Silica fume SEM images (left) and X-Ray Diffractogram pattern (right)

3.1.6 EMULSION PREPARATION

To prepare the emulsions, water was used as a dispersion medium, water-soluble PVA as surfactant and PMHS as the dispersion phase. Silica fume was used to stabilize [48-50] and modify the emulsion using three different approaches: simple, “shell” and “core” as described in CFIRE report 04-09 [51]. Additionally, Flores-Vivian *et. al.* (2013) [9] explained in detail the differences between these three emulsion concepts. The concentrations of surfactant, siloxane and silica fume were kept constant at 3.485, 25 and 5%, respectively, by the weight of the

emulsion, except for emulsion E_{1SR} (Table 5). E_{1SR} was produced by diluting 1 part of E_{1S} emulsion with 4 parts of DI water.

Table 5: Emulsion proportions

Emulsions ID Materials	Reference	E_1		
		(Core)	(Shell)	(Shell)
	E_0	E_{1C}	E_{1S}	E_{1SR}
DI water, %	71.215	66.215	66.215	80
PVA, %	3.485	3.485	3.485	0.697
Siloxane, %	25	25	25	5
Silica Fume, %	0	5	5	1
Biocide, %	0.3	0.3	0.3	0.06
Total, %	100	100	100	100

The water-soluble PVA swells quickly in water and has a tendency to clump together. To avoid clumping, PVA powder was gradually added to de-ionized water and stirred for 10 minutes at $23\pm 3^\circ\text{C}$, using a magnetic stirrer on a hot plate. Then, to achieve the complete dissolution, the temperature was increased to $95\pm 2.5^\circ\text{C}$, and kept constant for 40 minutes while stirring. The solution was allowed to cool in a water bath until a temperature of $23\pm 3^\circ\text{C}$ was achieved. A high speed mixer (HSM, model L5M-A from Silverson) was used to prepare the emulsions. The mixing procedure for PMHS and silica fume in PVA solution is explained in Figure 13. To stabilize the plain emulsions (without particles), high speed/shear mixing at 10,000 rpm was used to produce a very small droplet size. Medium speed (5000 rpm) was used only when particles were added.

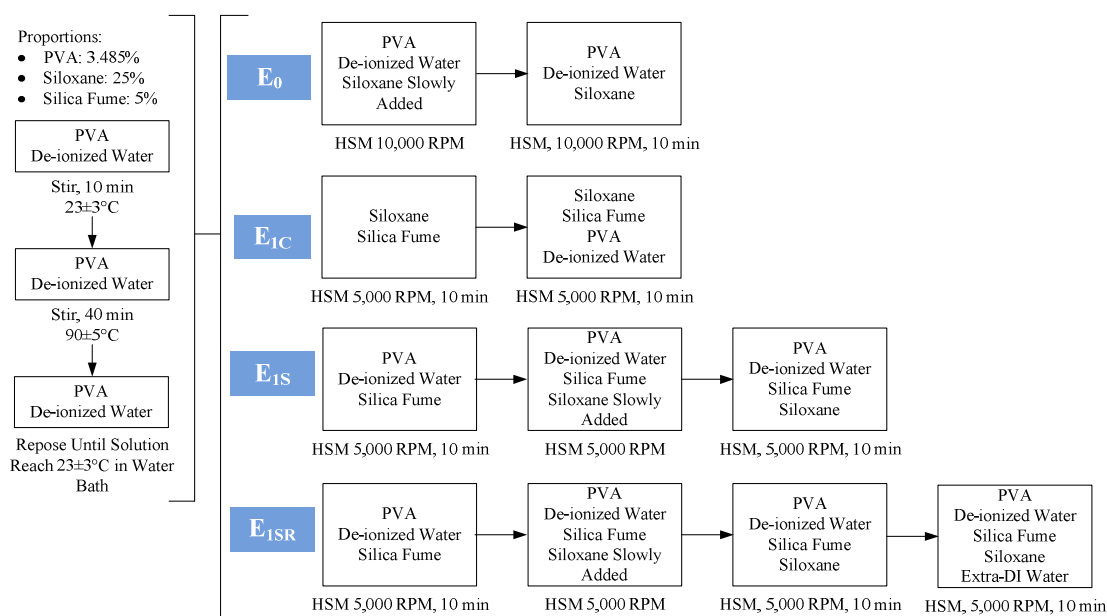


Figure 13: The procedure for preparation of emulsions

3.2 TYPE AND PREPARATION OF SPECIMENS

3.2.1 EMULSION TYPE EFFECT

The effect of cementitious phase fraction in the tiles, the type of emulsion and thickness of emulsion coating were studied in this section. Tile specimens produced with mortar mixes “B” and “C” were used to test the emulsion type effect on hydrophobicity by measuring water contact angles. The surface of the tiles was roughened with silicon carbide grinding paper with a grit of 320 for 1 minute in order to expose the fresh surface and sand aggregates. Polished tiles were washed with tap water to remove any particle contamination. Ultrasonic equipment, Hielscher model UIP1000hd, was used at 50% of maximal amplitude for 30 seconds to remove any loose particles from the surface of the tiles. The specimens were placed in an oven at 40 °C for 24 hours to remove any excess of water. Emulsions E₀, E_{1S} and E_{1C} with 25% of siloxane were used as coatings for the tiles. Three tiles for each mortar mix (B and C) were coated with 20, 40 and 80 µl (0.09, 0.18 and 0.35 l/m², respectively) of each emulsion. Specimens were allowed to cure at a room temperature for 48 hours before any contact angle measurement. The wetting properties of the tiles were examined by measuring the water contact angle using the Kruss DSA100 “Drop Shape Analysis System” goniometer. 20 µl of water was dosed onto each tile surface using the instrument’s automatic syringe.

3.2.2 MORTAR ROUGHNESS AND EMULSION DOSAGE EFFECT

The effect of mortar roughness and siloxane emulsion dosage was studied. Tile specimens produced using mortar “B” were used in the experiment. The surface of the tiles was roughened with silicon carbide paper with a grit of 60, 120 and 320 for 30 seconds in order to expose the fresh surface and sand aggregates. Polished tiles were washed with tap water to remove any surface contamination. Ultrasonic equipment, Hielscher model UIP1000hd, was used at 50% of maximum power for 30 seconds to remove any loose particles from the surface. The specimens were placed in an oven at 40 °C for 24 hours to remove any excess water. Emulsion E_{1SR} with 5% of siloxane was used as the coating. The mortar mix B tiles with different roughness treatments were coated with 5, 10, 20, 30, 40 and 50 µl (0.02, 0.04, 0.09, 0.13, 0.18 and 0.22 l/m², respectively) of emulsion. The specimens were allowed to dry at a room temperature for 48 hours before testing. The wetting properties of the tiles were examined by measuring the water contact angle using the Kruss DSA100 “Drop Shape Analysis System” goniometer. 20 µl of water was dosed onto each tile surface using the instrument’s automatic syringe.

3.2.3 SPLITTING TEST FOR ICE ADHESION

Two sets of mortars were prepared for the preliminary study of ice adhesion using cube specimens. Mortar (Mixture A) with higher aggregates content and mortar (Mixture B) with moderate aggregates content labeled as W1 and W2, respectively, were produced. Using a universal testing machine (Instron 3369) with a frame for splitting strength, cubes were crushed in half, producing two half-cube specimens, each with a fractured surface (Figure 14).



Figure 14: The set up for the specimen test (left), crushed specimens (center), and specimens treated with hydrophobic agent and bonded ice (right)

Surface coating was performed by completely soaking the mortar half-cube specimens in E_0 emulsion for 30 minutes. The specimens were allowed to dry for 48 hours in ambient room conditions and the contact angle measured on the treated and untreated fractured surfaces. Each mortar half-cube was then returned to its 50 mm cube mold and water was poured into the void space in the mold, such that the water was in contact with the fractured mortar surface (treated and untreated). These half-mortar, half-water cube molds were placed in a freezing room at -10°C degrees for 48 hours. The proportions of the specimens and coating treatments are shown in Table 6.

Table 6: The specimen mixture proportioning and icephobic treatment

Specimen ID	W/C	S/C	Treatment
W1-a	0.7	5.5	Uncoated
W1-b			Coated
W2-a	0.5	2.75	Uncoated
W2-b			Coated

Ice adhesion tests, determined by the splitting strength, were performed using a universal testing machine (Instron 3369) with a pace rate of 0.06 kN/s (0.0135 kip/s). The maximum splitting strength was determined using the equation analyzed by Timoshenko *et al.* (1951) [52] and confirmed by Davies and Bose *et al.* (1968) [53] for concrete cube specimens. Mortar specimens with bonded ice were tested according to the setup in Figure 15.

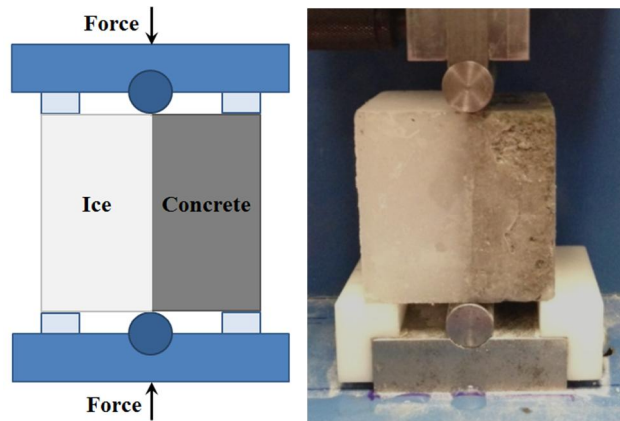


Figure 15: Setup of the splitting test

3.2.4 HYDROPHOBICITY AND ICEPHOBICITY TESTING

The effects of fibers, superhydrophobic coating, as well as the concentration of the hydrophobic agent (emulsion type) were investigated. Tile specimens produced using mortar mix series “M” was used in the experiment. The surface of the tiles was roughened with silicon carbide grinding paper with a grit of 60 for 30 seconds in order to expose the fresh surface and sand aggregates. Polished tiles were washed with tap water to remove any contamination from the surface. The aforementioned ultrasonic UIP1000hd was used at 50% of maximum power for 60 seconds to remove any loose particle from the surface of the tiles. Specimens were placed in an oven at 40 °C for 24 hours to remove any excess of water. Emulsions E_{IS} and E_{ISR} with 25 and 5% of siloxane, respectively, were used as coating material on the tiles at a surface dose volume of approximately $10 \mu\text{l}$ (0.04 l/m^2). The specimens were allowed to dry at a room temperature for 48 hours before contact angle measurements were made. The wetting properties of the tiles were examined by measuring the water contact angle using the Kruss DSA100 “Drop Shape Analysis System” goniometer. $20 \mu\text{l}$ of water was dosed onto each tile surface using the instrument’s automatic syringe.

In the preliminary work, fractured cubes were used to test the ice adhesion. Due to their irregular surface and in order to control the dosage of the hydrophobic emulsion, the tile specimens as described in the previous section were used to measure the ice adhesion shear strength. Mortar specimens and stainless steel cylinders (Figure 16, top-left) with an inner diameter of 11 mm were kept at $-10 \text{ }^\circ\text{C}$ for at least 2 hours. Tap water, stored at $0.4 \text{ }^\circ\text{C}$ for at least 2 hours, was placed into the pre-chilled cylinders set on the treated surface of the tiles. Sealer was not used between the cylinder and the tile because water was immediately solidified within the cylinder (Figure 16, bottom-left). Mortar specimens with bonded ice were tested using the setup of Figure 16 (right). The ice adhesion was tested using the stress-strain apparatus (Pasco CI-6746) with a pace rate of approx. 60 rpm. Applied load and extension of the ice block were recorded for shear strength calculation and plotting. Shear strength was determined using the load recorded and the inner area of the cylinder using the equation $\tau = F/A$.



Figure 16: The specimen preparation for the ice adhesion tests (left and center) and the setup for the test (right)

4. EXPERIMENTAL RESULTS AND DISCUSSION

4.1 PRELIMINARY STUDIES

4.1.1 SCREENING OF SILANE AND SILOXANE COMPOUNDS

Commercially available silane and siloxane based chemicals were examined for their effectiveness in imparting hydrophobicity and icephobicity to concrete based materials. The results for contact angle (theta mean) and percent ice loss are summarized in Table 7. The plot of Ice loss on impact vs. contact angle is shown in Figure 17. In terms of contact angle, the best performers were from polymethyl-hydrogensiloxane at 131° and n-octyltrieth-oxysilane at 124° . n-Octyltrieth-oxysilane also had the highest % ice loss at 94%, followed by sodium methyl silicate at 84%. Though it did not give the very best contact angle, sodium methyl silicate remained compelling, since it is water soluble and it was still a good performer in the group. One would have expected potassium methyl silicate to behave similarly to the sodium salt, and it did in terms of contact angle; percent ice loss was much less, however, at 46% vs. 84% for the sodium salt. This may say more about the preliminary version of the percent ice loss test than the material itself, particularly since one repetition was done. Though the correlation coefficient was 0.44, there was a general trend with icephobicity (via percent ice loss) increasing with hydrophobicity (via contact angle). The test itself gave some compelling results, which warrant further work.

4.1.2 THE EFFECT OF MORTAR AND EMULSION TYPE

The effect of the cementitious fraction in the type of emulsion and quantity of emulsion coating were studied in this section (Figure 18). The highest contact angles were observed when the dosage of emulsion was increased and when the fraction of the cementitious material was reduced (Mix B). A reduction of the cementitious material volume demonstrated that the roughness induced by sand is an important parameter affecting hydrophobicity, as the higher the roughness the greater the contact angle achieved.

Table 7: The effect of the agent on hydrophobicity and ice adhesion

Tile ID	Siloxane/silane active treatment	Ice drop weight	Ice loss, %	Contact angle, deg
A00	Untreated/Reference	0.117	47%	8
A01	Polymethylhydrogensiloxane	0.136	77%	131
A02	Polydimethylsiloxane, 200 cSt	0.141	60%	85
A03	Polydimethylsiloxane, 300 cSt	0.134	70%	121
A04	t-Butyltrimethoxysilane	0.135	78%	124
A05	N-(3-(Trimethoxysilyl)propyl)ethylenediamine *	0.135	57%	85
A06	Methyltrimethoxysilane	0.134	69%	121
A07	Hexamethyldisilazane	0.138	28%	65
A08	Phenyltrimethoxysilane	0.136	69%	114
A09	Aminosilsesquioxanes. methoxy-terminated *	0.139	60%	72
A10	Vinyltrimethoxysilane	0.141	78%	123
A11	n-Octyltriethoxysilane	0.134	94%	124
A12	Tetraethoxysilane	0.140	65%	70
A13	Sodium methyl siliconate	0.135	84%	111
A14	Potassium methyl siliconate	0.133	46%	113

* Primary component in alkoxy silane blend

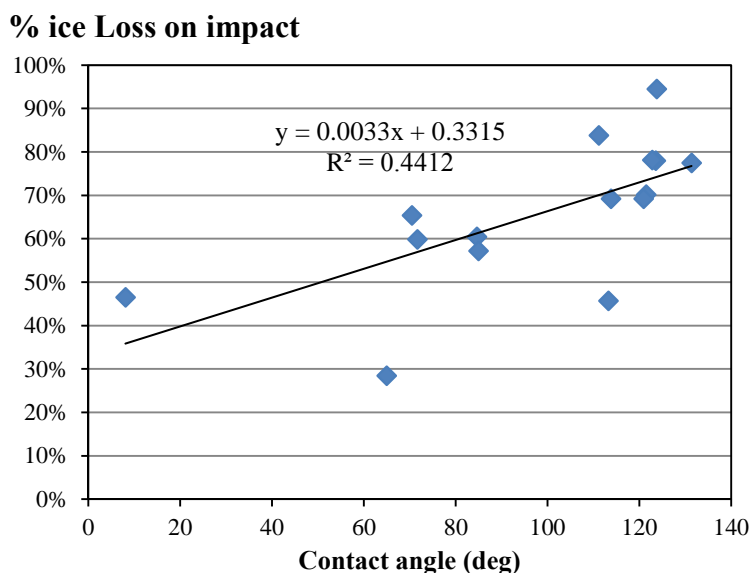


Figure 17: The relationship between the ice loss and contact angle

The lowest roll-off angles were observed on the tile specimens with a higher fraction of cementitious material (Mix C) when emulsions with silica fume were used. The E_0 emulsion demonstrated reduced contact angle measurements relative to the E_{1S} and E_{1C} emulsions with silica fume. The highest roll-off angles were also observed for E_0 emulsion. The addition of fine particles was demonstrated to have a positive effect on the hydrophobicity of the emulsions. Agglomeration and a poor dispersion of fine particles were observed during the production of core emulsions (E_{1C}). Flores-Vivian *et. al.* (2013) [9] demonstrated that “core” and “shell” emulsions can be produced with small volumes of fine materials (0.5%) [9]. In this research,

higher quantities of ultra-fine materials were used (5%) which affected the mixing effectiveness for core emulsions. The shell emulsions (E_{1S}) were selected for further studies.

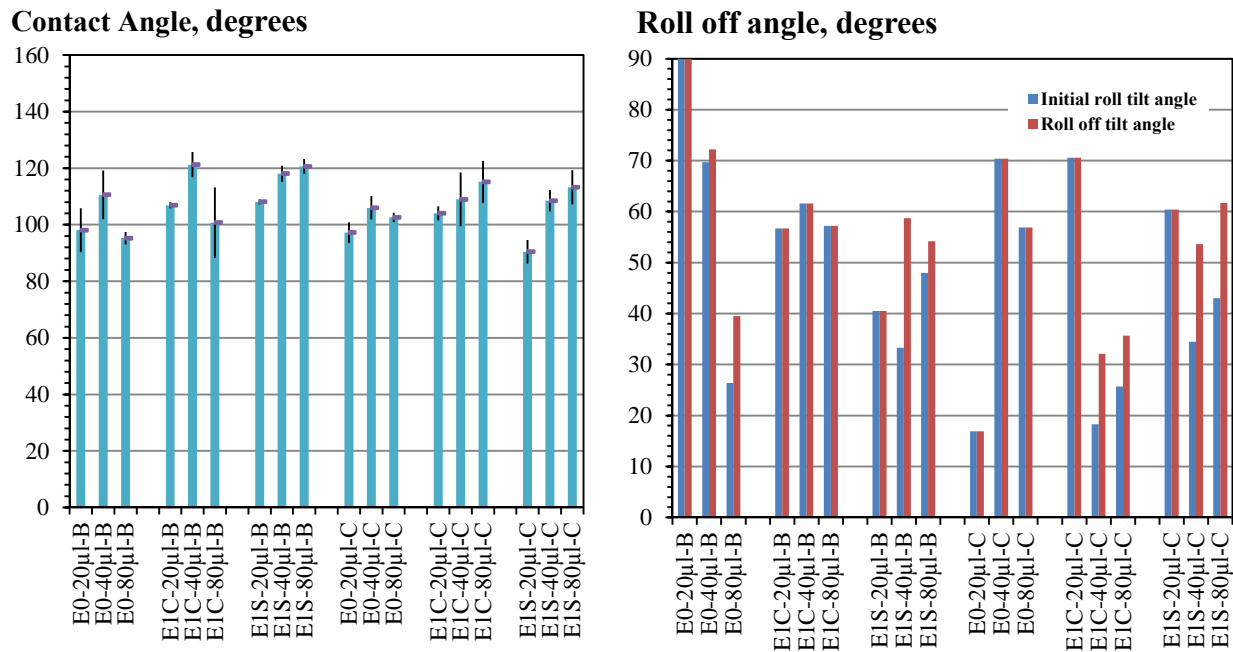


Figure 18: The contact angles (left) and the roll-off angles (right) for tiles coated by different emulsions

4.1.3 THE EFFECT OF MORTAR ROUGHNESS AND EMULSION

The effect of mortar roughness and quantity of siloxane emulsion were studied in this section (Figure 19). Emulsion E_{1SR} with 5% of siloxane were used to coat the tiles. These emulsions increased the average contact angle by 10° over E_0 , E_{1S} , and E_{1C} emulsions as studied in the previous section. The same effect was observed for the roll-off angle. When 60-grit sandpaper was used, the contact angle fell as emulsion dosage was incrementally reduced. When 320-grit sandpaper was used to induce roughness, an optimal contact angle was obtained when $30 \mu\text{l}$ (0.13 l/m^2) of the emulsion was used for coating. Additionally, a reduction of the roll-off angle was observed when 320-grit sandpaper was used. The studies performed with 120-grit sand paper demonstrated good results; however, they were not conclusive with respect to the emulsion dosage. Considering the values from the previous section (4.1.2), where 25% siloxane was used, the best results were achieved with a siloxane concentration of 5%, and therefore E_{1SR} was selected for further studies. The lower viscosity of E_{1SR} emulsion, enhancing its flow over the surface, may be a reason for higher contact angles as compared to other emulsions.

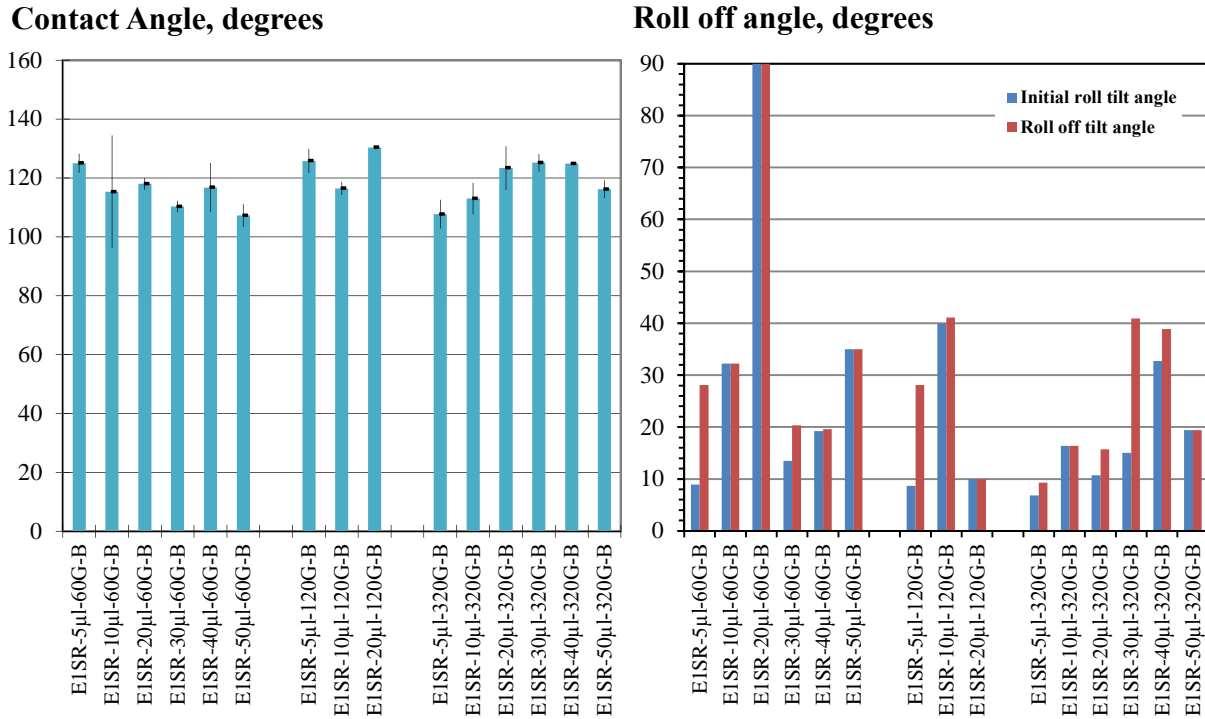


Figure 19: Contact angles (left) and roll-off angles (right) for tiles with different roughness and volume of emulsion coating

4.1.4 CONTACT ANGLE TESTS FOR THE ICE ADHESION STUDY

The contact angles measurements for the tiles coated with icephobic emulsions are shown in Figure 20. Uncoated tiles were also prepared and tested for contact angle; however, due to the high porosity of the specimens, no contact angle measurements were recorded (since all water was absorbed by the specimen). Higher contact angle measurements were observed for the specimens with higher content of sand (W1). Here, the higher content of aggregates enhances the roughness of the mortar surface. Higher roughness in W1 specimens produced a hierarchical surface, increasing the contact angle by 5 degrees.

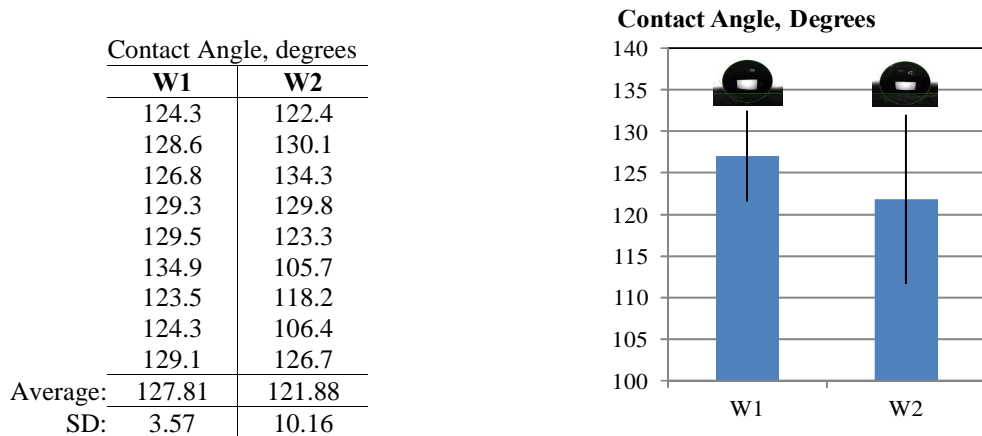


Figure 20: The contact angle of coated tiles

4.1.5 ICE ADHESION: SPLITTING STRENGTH

The applied load and deformation (extension) of uncoated and coated specimens W1 and W2 tested for splitting strength are shown in Figure 21 and Figure 22 respectively. The maximum load and extension were reduced by 18 to 21% and 5 to 29 %, respectively, when the fractured surface was coated with the hydrophobic emulsion. The specimens with higher S/C ratios demonstrated a reduced bond with ice because of a lower cement paste contact area available for adhesion.

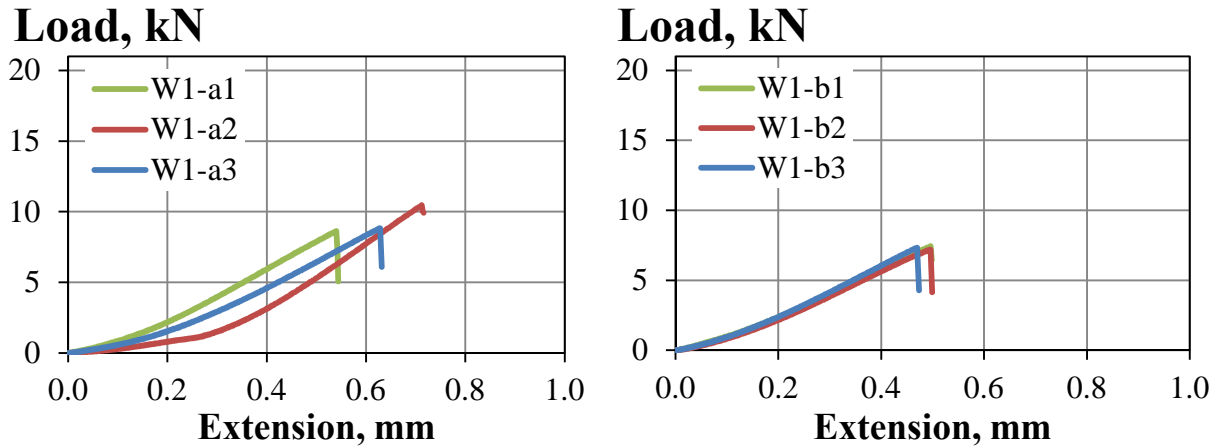


Figure 21: Load vs extension for uncoated (left) and coated (right) W1 ($w/c=0.7$; $s/c=5.5$) specimens

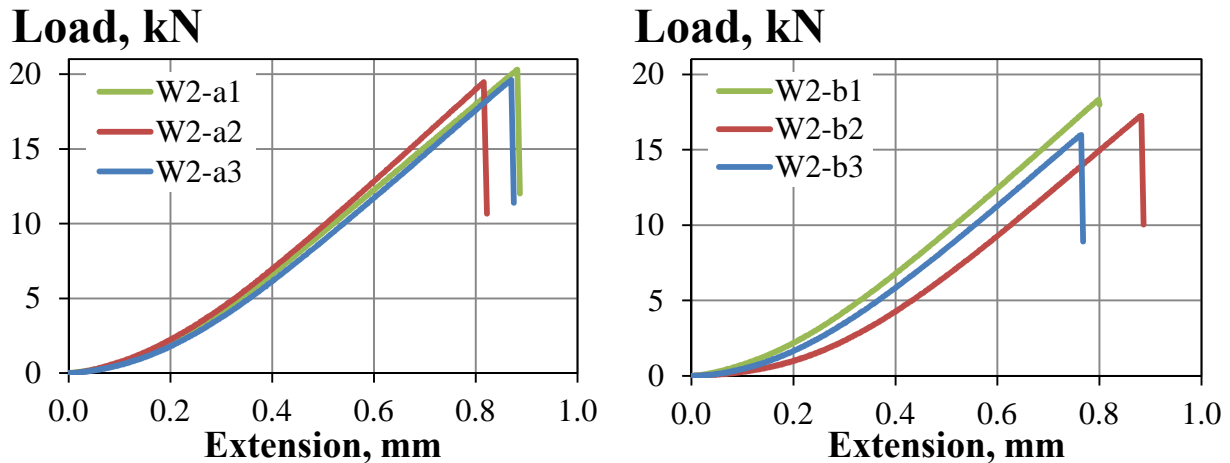


Figure 22: Load vs. extension for uncoated (left) and coated (right) W2 ($w/c=0.5$; $s/c=2.75$) specimens

In all cases, the emulsions helped to reduce the ice adhesion to treated fractured surfaces, where the ice adhesion was relatively weak, inducing separation at the bonding area. In contrast, the fracture of ice itself was observed for uncoated specimens (Figure 23). The maximum load and extension are reported in Table 8 for all tests. The contact area for ice adhesion was considered to be the cross sectional area of the cube and splitting strength was calculated for all specimens using this assumption. The reduction in the ice bond splitting strength was observed in specimens with a low fraction of cementitious matrix so the specimens with higher W/C and S/C

ratios had a 50% lower splitting strength. In this way, aggregate proportions play an essential role in ice adhesion, sometimes dominating the effects of hydrophobic treatment.

Table 8: Splitting strength for coated and uncoated specimens

Specimen ID	Pace rate, kN/s	Max. Extension, mm			Av. Max. Extension, mm	Max. Load, kN			Av. Max. Load, kN	Area, mm ²	Splitting Strength, MPa
W1	0.06	0.543	0.712	0.628	0.628	7.01	10.46	8.83	8.77	2590.8	2.15
W1-S	0.06	0.496	0.496	0.470	0.487	7.43	7.19	7.32	7.32	2590.8	1.80
W2	0.06	0.816	0.870	0.882	0.856	19.47	19.61	20.31	19.79	2590.8	4.86
W2-S	0.06	0.764	0.798	0.882	0.815	15.99	18.31	17.26	17.18	2590.8	4.22

The observed reduction of the ice bond for mortars with a lower fraction of cementitious matrix can be explained by:

- lower surface of cementitious matrix available for bond with ice and aggregates shielding the specimen
- weaker matrix allowing the debond of the aggregates grains when the load is applied
- rough surface, so the hydrophobic effects are enhanced, as seen in the contact angle measurements
- higher porosity, enabling better absorption of hydrophobic emulsions, and preventing defects on the hydrophobic coatings



Figure 23: The ice fracture patterns of uncoated (left) and coated (right) specimens

4.2 THE EFFECT OF FIBERS

The effects of fibers, the concentration of cementitious material, and the concentration of the hydrophobic agent (emulsion type) were investigated. Emulsions E_{1S} and E_{1SR} with 25 and 5% of siloxane, respectively, were used for coating of the tiles (Figure 24). Due to the high water absorption, the contact angles for uncoated specimens were very small, from 0 to 20 degrees. Uncoated specimens absorb most of the water since Portland cement based materials are hydrophilic. The contact angles were comparable to the preliminary results on plain mortars without fibers. The contact angle of coated specimens was approximately 10 times that of uncoated specimens and an additional gain of approximately 15 degrees was realized when E_{1SR} was used. The addition of fibers increased the contact angles for all specimens. A further increase in fiber content may improve the hydrophobicity of the surface producing a superhydrophobic surface. The hydrophobic properties of treated surfaces were highly evident when the roll-off angle was measured (Figure 25). No roll off angle was recorded for uncoated specimens because the water was completely absorbed by the tiles.

Contact angle, degrees

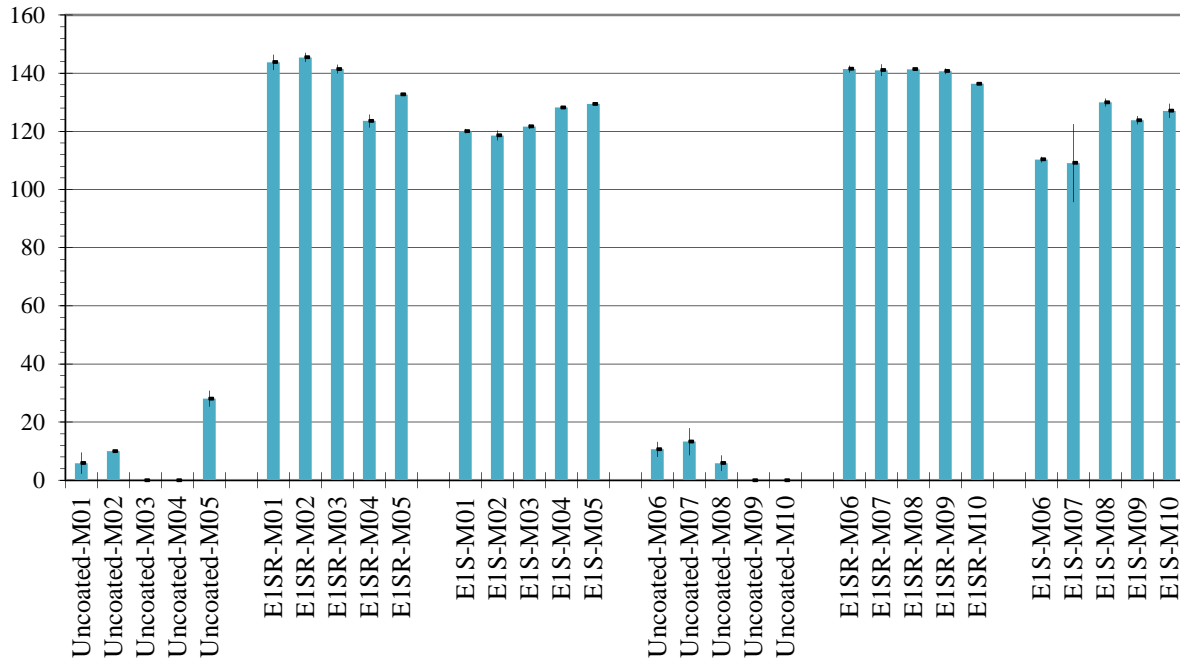


Figure 24: The contact angle for tiles coated by E_{1S} and E_{1SR} emulsions.

Tilt angle, degrees

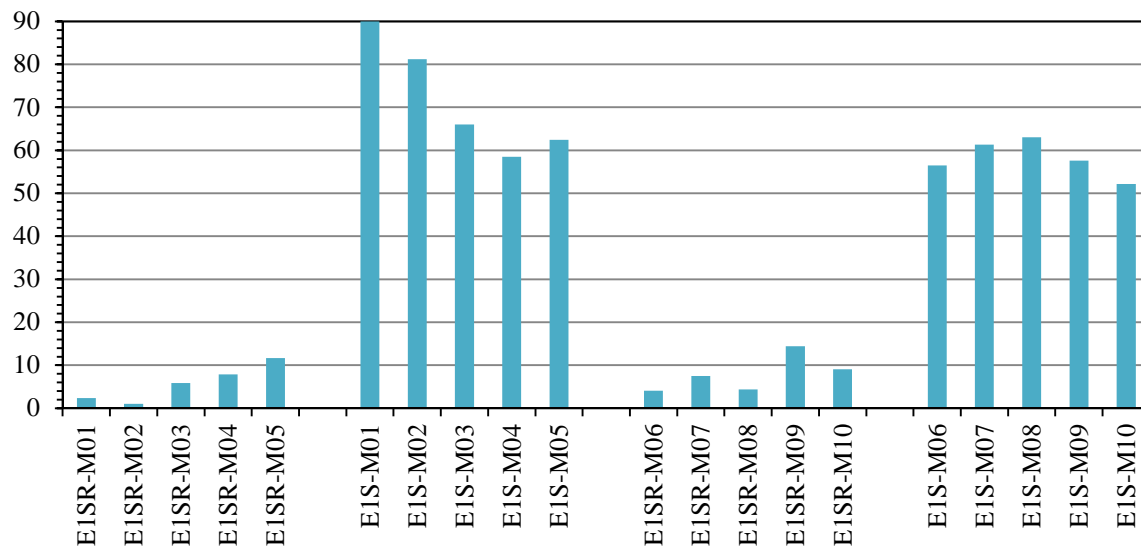


Figure 25: Roll-off angles for tiles coated by E_{1S} and E_{1SR} emulsions.

The concentration of the cementitious material had a smaller effect on the roll-off angle than the type of the emulsion. Roll-off angles of specimens with E_{1S} emulsion were in the range of 50 to 65 degrees, while E_{1SR} values were 6 times lower, in the range of 4 to 15 degrees. For the specimens coated with E_{1S} , the contact angle increased with the reduction of the cementitious fraction. The roughness introduced by the aggregates increased the hydrophobicity of tiles coated

by E_{1S} . On thicker coats, the higher roughness induced by the aggregates had a positive effect on the hydrophobicity of the material. The higher concentration of hydrophobic agent in E_{1S} seemed to minimize the roughness effect of the fibers. The diluted emulsion E_{1SR} developed a thin coat, which allows fibers to play a major roll on the hydrophobicity and superhydrophobicity of the specimens.

4.3 ICE ADHESION BY SHEAR TESTING

The tile specimens were used to measure the ice adhesion strength. The ice adhesion characteristics of specimens with fibers are shown in Figure 26. All uncoated tiles presented a higher ice bond relative to coated specimens. The shear stress required to remove ice from the surface was in the range of 0.18 to 0.33 MPa for uncoated and 0.03 to 0.12 MPa for coated specimens. The average values for maximum shearing strength for uncoated and coated tiles were 0.25 and 0.05 MPa, respectively. Consequently, coated specimens can be expected to have ice shear bond reduced to one sixth that of uncoated tiles.

The corresponding shearing strength plots for specimens without fibers are shown in Figure 27. All uncoated tiles had higher ice bonds versus coated specimens. The shear stress required to remove ice from the surface was in the range of 0.18 to 0.31 MPa for uncoated and 0.02 to 0.07 MPa for coated specimens. The average maximum shearing strengths for uncoated and coated tiles were 0.26 and 0.05 MPa, respectively. On average, coated specimens presented a reduced shearing strength, one fifth that of uncoated tiles.

The ice adhesion shear strength was reduced when fibers were used. The ice adhesion was successfully measured by the proposed method. A correlation between the maximum ice adhesion shear strength and the hydrophobic properties of the coating (contact angle) are shown in Figure 28. Appendix 3 has the average values used to plot graphs in Figure 28. It was observed that the higher the contact angle of the hydrophobic coat, the lower the shear stress needed to break the bond. The same effect was observed when the roll-off angle was reduced.

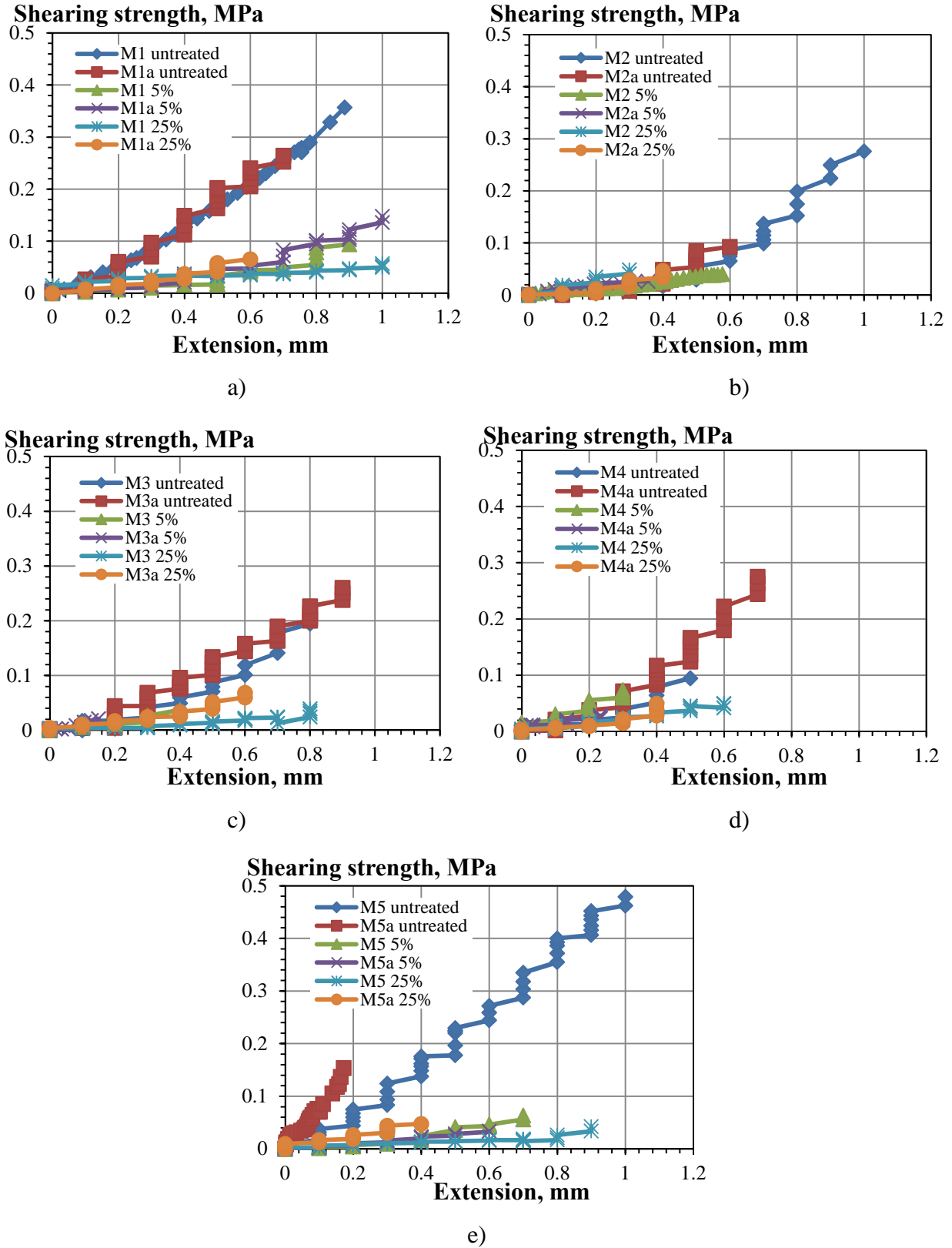


Figure 26: The shear strength (ice adhesion) of specimens with fibers: a) M1, b) M2, c) M3, d) M4, and e) M5.

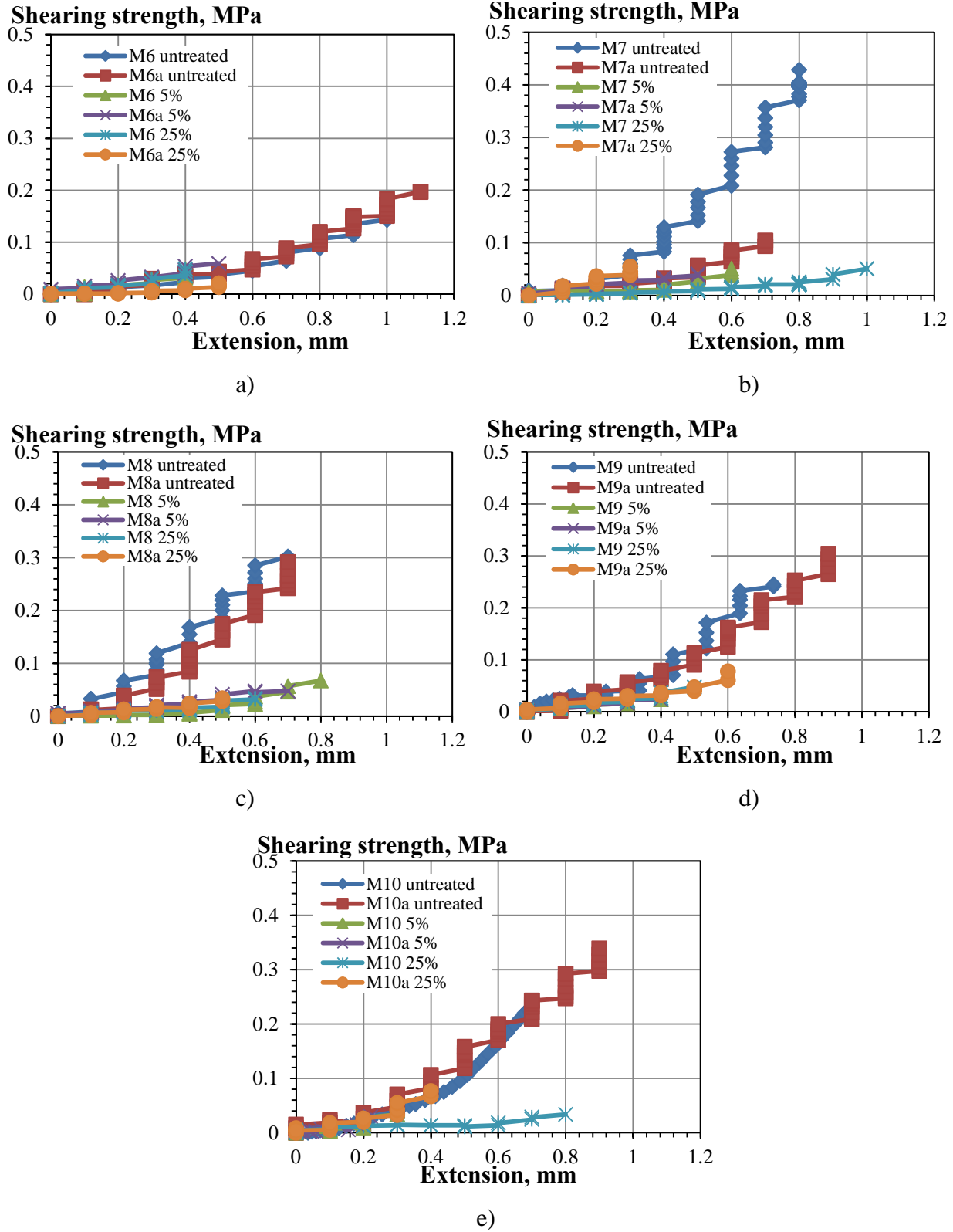


Figure 27: The shear strength (ice adhesion) of plain specimens (without fibers): a) M6, b) M7, c) M8, d) M9, and e) M10.

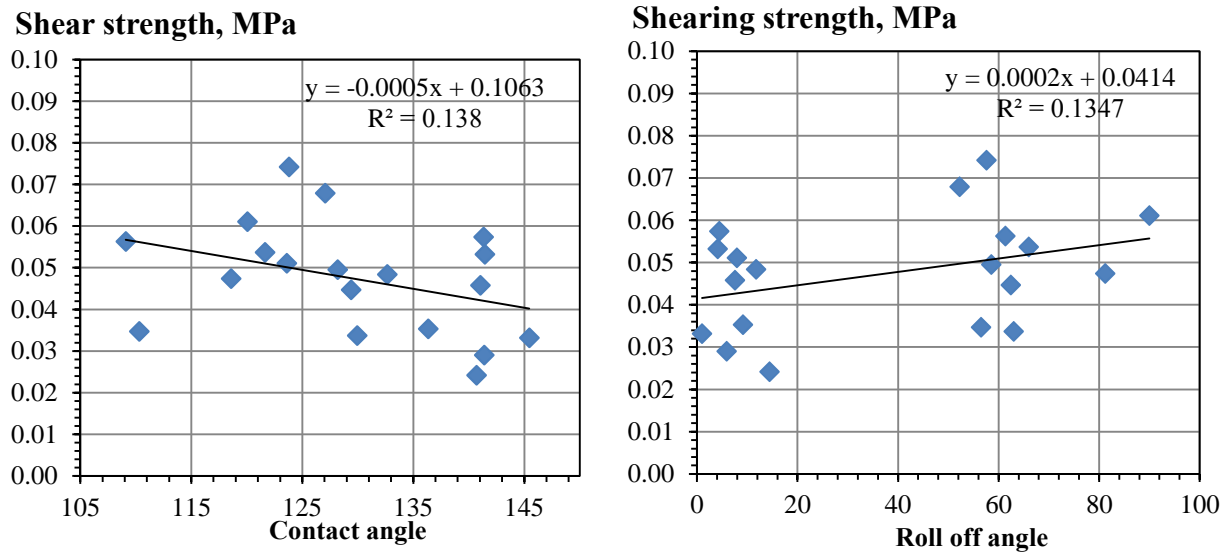


Figure 28: The correlation between the maximum shear strength and contact (left) or roll-off (right) angle

5. CONCLUSIONS

A new icephobic concrete is proposed to reduce the ice adhesion on roadway pavements and bridges. The proposed method involves the engineering of the hierarchical structure for concrete wearing surface by optimization of aggregates, the use of fibers, and the application of superhydrophobic siloxane admixtures. The superhydrophobic admixture is based on a combination of siloxane-based hydrophobic liquid and small quantities of super-fine materials such as silica fume. The research demonstrated that the best water repellent materials (measured by the contact angle) were obtained using polymethyl-hydrogen-siloxane. Preliminary studies on mortars (without fibers) demonstrated that the ice adhesion strength can be measured using different methods. The most reliable procedure involved a shear test to remove the ice from mortar tiles.

Extensive tests on hydrophobicity and ice adhesion were performed using siloxane treatments on mortars with and without fibers. Uncoated mortar tiles absorb much of the water resulting in higher ice adhesion, with up to 0.33MPa. Coated mortar tiles effectively repel water, where the fiber content, the concentration of the hydrophobic additive and the fraction of the cementitious material were the key factors. Among these, the addition of fibers and the dilution of the emulsion were the parameters that greatly enhance the hydrophobicity. Diluted emulsions (5% active material) allow the fiber to produce a hierarchical surface of fibers and aggregates so the material behaves like a superhydrophobic coat. This enables the treated specimens to have a very weak ice adhesion with the shear strength in the order of 30 kPa, which is one tenth of that of untreated specimens.

The superhydrophobic approach to concrete material enhancement creates an icephobic material by reducing the ice bond strength so that ice is removed easily from the road surface. This can reduce the fatalities, injuries and property losses associated with winter driving, ensuring the efficiency of freight even in challenging road conditions. Since water is not allowed to penetrate concrete, freeze-thaw and corrosion resistance can be enhanced. The developed material can provide a much extended lifespan for critical elements of bridges and other transportation infrastructure. Moreover, the use of icephobic materials in highway infrastructure can significantly reduce the need for maintenance. With increasing costs for de-icing and anti-icing materials currently used on highways, and considering new environmental regulations, the need for new icephobic cementitious composites which can provide the required durability and mechanical response for critical elements of transportation infrastructure is evident.

6. FUTURE WORK

The results of the reported research can be used to manufacture a new-generation of overhydrophobic and superhydrophobic concrete materials with the enhanced icephobicity required for critical components of infrastructure such as highway bridges. The effects of higher fiber contents must be investigated to enhance the hydrophobicity of the concrete and reduce ice adhesion. An abrasion resistance investigation is required to understand the life cycle of the icephobic coatings and the effects of freezing and thawing exposure must be addressed. Field tests on roadways are desired to understand the benefits and disadvantages of icephobic concrete proposed in this research.

7. REFERENCES

1. Icy Road Safety, www.icyroadsafety.com
2. Robinson, Rhonda; Jones, Stan, "Ice detection and avoidance," *International Oil Spill Conference, IOSC 2005*, p 9570-9573, 2005.
3. Robert R. Blackburn, Karin M. Bauer, Duane E. Amsler, S. Edward Boselly, A. Dean McElroy, Snow and Ice Control: Guidelines for Materials and Methods, NCHRP REPORT 526, Transportation Research Board, 2004.
4. Stephen A. Ketcham, L. David Minsk, Robert R. Blackburn, Edward J. Fleege, Manual of Practice for an Effective Anti-Icing Program-Guide for Highway Winter Maintenance Personnel, US Army Cold Regions Research and Engineering Laboratory Corps of Engineers, 1996.
5. Eli Cuelho, Jason Harwood, Michelle Akin and Ed Adams, Establishing Best Practices of Removing Snow and Ice from California Roadways, Report No. CA10-1101, Western Transportation Institute - Montana State University, December 2010
6. Using Salt and Sand for Winter Road Maintenance, Wisconsin Transportation Bulletin • No. 6 August 2005 http://epdfiles.engr.wisc.edu/pdf_web_files/tic/bulletins/Bltn_006_SaltNSand.pdf
7. Liu, Y. (2006). Super hydrophobic surfaces from a simple coating method: A bionic nanoengineering approach. *Nanotechnology*, 17, 3259-3263.
8. M Nosonovsky, 2007, Multiscale roughness and stability of superhydrophobic biomimetic interfaces *Langmuir* 23 (6), 3157-3161
9. Ismael Flores-Vivian, Vahid Hejazi, Marina Kozhukhova, Michael Nosonovsky, Konstantin Sobolev, Self-assembling particle-siloxane coatings for superhydrophobic concrete, *ACS Applied Materials & Interfaces*, 2013, *in press*
10. Sobolev K. and Ferrada-Gutiérrez M., How Nanotechnology Can Change the Concrete World: Part 2. *American Ceramic Society Bulletin*, 11, 2005, 16-19.
11. Sobolev K. and Batrakov V., The Effect of a PEHSO on the Durability of Concrete with Supplementary Cementitious Materials. *ASCE Journal of Materials in Civil Engineering*, 19(10), 2007, 809-819.
12. Becky Poole, Biomimetics: Borrowing from Biology <http://www.thenakedscientists.com/HTML/articles/article/biomimeticsborrowingfrombiology/>
13. M. Nosonovsky, "Slippery when wetted" *Nature* 477 (2011) 412-413
14. M. Nosonovsky, B. Bhushan, "Superhydrophobic Surfaces and Emerging Applications: Non-adhesion, Energy, Green Engineering," *Current Opinions Coll. Interface Sci.* 14 (2009) 270-280
15. V. Hejazi, K. Sobolev, M. Nosonovsky, "From superhydrophobicity to icephobicity: forces and interaction analysis" *Nature's Sci. Rep.* (2013) 3:2194
16. Moriconi, G., Tittarelli, F. (2009). Effectiveness of surface or bulk hydrophobic treatments in cementitious materials. *Protection of Historical Buildings, PROHITECH*, 09, 1071-1075.
17. Raupach, M., Wolff, L. (2005). Investigations on long-term durability of hydrophobic treatment on concrete. *Surface Coatings International PartB: Coatings Transactions*. 99(2), 127-133.
18. Popovics, S. (1982). *Fundamentals of portland cement concrete, Vol. 1: Fresh Concrete*, John Wiley and Sons Inc

19. Hekal, E. E., and Abd-El-Khalek, M. (1999). Mechanical and physico-chemical properties of hardened portland cement pastes containing hydrophobic admixtures part 1: Compressive strength and hydration kinetics. *Zkg International*, 52(12), 697-700.
20. Hekal, E. E., and Abd-El-Khalek, M. (2000). Mechanical and physico-chemical properties of hardened portland cement pastes containing hydrophobic admixtures part2: Physical properties and micro-structure. *Zkg International*, 53(3), 152-158.
21. Wacker. (2009). Concrete protection for concrete advantages. Wacker Silicones, Retrieved from http://www.wacker.com/cms/media/publications/downloads/6527_EN.pdf
22. De Vries, I., and Polder, R. B. (1995). Hydrophobic treatment of concrete. *Construction and Building Materials*, 11(4), 259-265.
23. Xiaojian G, Ying Z., (2011). Influence of Silane Treatment on the Freeze-Thaw Resistance of Concrete. *Advanced Materials Research*, 250, 565-568.
24. Batrakov, V. G. (1998). Modified concrete- theory and practice. Moscow, Russia: Stroyizdat.
25. Basheer, P. A. M., L. Basheer, et al. (1997). Surface treatments for concrete: Assessment methods and reported performance. *Construction and Building Materials*, 11(7-8), 413-429.
26. The National Cooperative Highway Research Program (NCHRP) report 244
27. Grubl, P., and M. Ruhl. "German Committee for Reinforced Concrete (DAfStb)-Code: Concrete with Recycled Aggregates." In *sustainable construction: use of recycled concrete aggregate-proceedings of the international symposium held at department of trade and industry conference centre, London, UK, 11-12 november 1998*.
28. Ibrahim, M., and Al-Gahtani, A. S. (1999). Use of surface treatment materials to improve concrete durability. *Journal of Materials in Civil Engineering*, 11(1), 36-40.
29. Tittarelli, F., Moriconi, G., Fratesi, R. (2000). Influence of silane-based hydrophobic admixture on oxygen diffusion through concrete cement matrix. *Superplasticizers and Other Chemical Admixtures in Concrete: Proceedings of the Sixth CANMET/ACI International Conference (SP-195)*, Nice, France.ed. V.M. Malhotra, American Concrete Institute, 431-445.
30. Fratesi, R., Moriconi, G., Tittarelli, R., & Collepardi, M. (1997). The influence of hydrophobized concrete on the corrosion of rebars. *superplasticizers and other chemical admixtures in concrete. Proceedings Fifth CANMET/ACI International Conference*, 105-122.
31. Menini, Richard, and Masoud Farzaneh. "Advanced Icephobic Coatings." *Journal of Adhesion Science and Technology* 25.9 (2011): 971-992.
32. Mulherin, N. D., and R. B. Haehnel. "Ice Engineering Technical Note, 03-4." (2003).
33. Sarshar, Mohammad Amin, et al. "Effects of Contact Angle Hysteresis on Ice Adhesion and Growth over Superhydrophobic Surfaces under Dynamic Flow Conditions." *Journal of Adhesion Science and Technology* 290.15 (2012).
34. Farhadi, S., M. Farzaneh, and S. A. Kulinich. "Anti-icing performance of superhydrophobic surfaces." *Applied Surface Science* 257.14 (2011): 6264-6269.
35. Kulinich, S. A., et al. "Superhydrophobic surfaces: are they really ice-repellent?." *Langmuir* 27.1 (2010): 25-29.
36. He, Min, et al. "Super-hydrophobic film retards frost formation." *Soft Matter* 6.11 (2010): 2396-2399.
37. Guo, Peng, et al. "Icephobic/Anti-Icing Properties of Micro/Nanostructured Surfaces." *Advanced Materials* 24.19 (2012): 2642-2648.

38. Kulinich, S. A., and M. Farzaneh. "Ice adhesion on super-hydrophobic surfaces." *Applied Surface Science* 255.18 (2009): 8153-8157.
39. Cao, Liangliang, et al. "Anti-icing superhydrophobic coatings." *Langmuir* 25.21 (2009): 12444-12448.
40. Laforte, Caroline, and Arlene Beisswenger. "Icephobic material centrifuge adhesion test." *Proc 11th International Workshop on Atmospheric Icing of Structures, Montréal*. 2005.
41. Zou, M., et al. "Effects of surface roughness and energy on ice adhesion strength." *Applied Surface Science* 257.8 (2011): 3786-3792.
42. ASTM C150, American Society for Testing and Materials; Standard specification of portland cement; ASTM C150; 2012; 4.01.
43. ASTM C778, American Society for Testing and Materials; Standard specification of standard sand; ASTM C778; 2013; 4.01.
44. ASTM C305, American Society for Testing and Materials; Standard Practice for Mechanical Mixing of Hydraulic Cement Pastes and Mortars of Plastic Consistency; ASTM C305; 2013; 4.01
45. ASTM C109, American Society for Testing and Materials; Compressive Strength of Hydraulic Cement Mortars (Using 2-in or 50-mm Cube Specimens); ASTM C109; 2012; 4.01.
46. Kim, J. H., & Robertson, R. E. (1999) Structure and properties of poly(vinyl alcohol)-modified mortar and concrete. *Cement and Concrete Research*, 29(3), 407-415.
48. Binks B. P. and Lumsdon S. O., (2000) Influence of Particle Wettability on the Type and Stability of Surfactant-Free Emulsions, *Langmuir* 16 (23), pp 8622-8631.
49. Aveyard R., Binks B.P., Clint J.H., (2003) Emulsions stabilised solely by colloidal particles, *Advances in Colloid and Interface Science*, Vol. 100-102, 28 February, pp. 503-546.
50. Ngai T., Auweter H., and Behrens S.H. (2006) "Environmental responsiveness of microgel particles and particle-stabilized emulsions." *Macromolecules*, 39.23, pp. 8171-8177.
51. Superhydrophobic Engineered Cementitious Composites for Highway Bridge Applications: Phase I; National Center for Freight & Infrastructure Research & Education; CFIRE 04-09; University of Wisconsin-Milwaukee, University of Wisconsin-Madison; May 2013.
<http://www.wistrans.org/cfire/research/projects/04-09/>
52. Timoshenko S. and Goodier J.N., (1951) *Theory of elasticity*, McGraw-Hill Book Co. New York, 2nd Edition, p. 107.
53. Davies J.D. and Bose D.K., (1968) Stress distribution in splitting tests, *American Concrete Institute*, August, p. 662-669.

APPENDIX A: FALLING ROD IMPACT TEST AND PROCEDURE

The falling rod test was developed for quantification of ice removal via physical impact. For this test, a water droplet was applied to a 15x15x8 mm tile. The tile and water were held in a chilled environment, generating frozen ice droplet. The method of ice removal was a falling rod striking ice droplet, with the amount of ice removed being a measure of icephobicity (Figure A1).

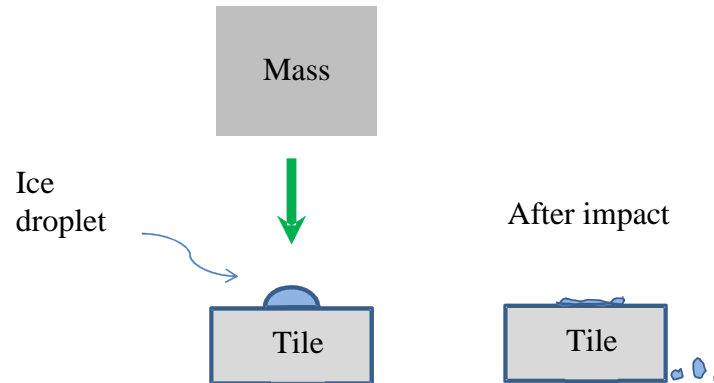


Figure A1: Ice loss on physical impact concept

Apparatus: Laray falling rod

The apparatus used for falling rod impact was a Laray falling rod viscometer, shown in Figure A2. The Laray viscometer is normally used to measure the viscosity of paste-like inks and fluids and comes equipped with a two photoelectric switches spaced 10 cm apart to enable the calculation of rod speed.



Figure A2: Laray falling rod viscometer apparatus with timer

For the ice impact application, the falling rod drop-time consistently measured 0.1 sec for 0.1 m at freezer temperatures of -10 deg C and -20 deg C, corresponding to 1.0 m/sec rod velocity (Figure A3).

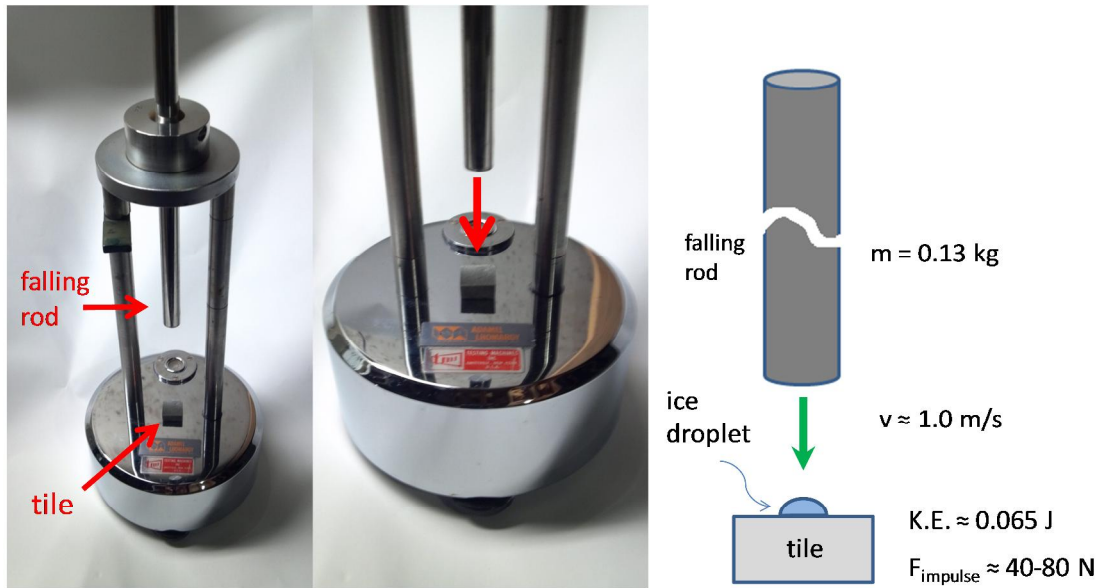


Figure A3: Ice adhesion via physical impact falling rod

APPENDIX B: FALLING ROD IMPACT TEST SAMPLE PREPARATION AND TEST

Sample preparation: casting of ice on tile

The deionized water used for ice casting and the micropipette were allowed to equilibrate to $+10 \pm 3$ °C for a minimum of 1 hour in a buffer room outside the freezer. Before dosing water, the micropipette was set for 150 microliters and adjusted if needed so that its dosage, as weighed on the analytical balance, was 0.150 ± 0.010 g of water at $+10 \pm 3$ °C. In the freezer, nominally 150 microliters of water was dosed on each pre-equilibrated and leveled tile using the preset micropipette (Figure B1). In order to prevent micropipette icing and contraction, no more than 6 droplets at a time were dosed. The water and micropipette were returned to the buffer room for 1-2 minutes before dosing water again. The tiles with ice droplets were allowed to chill for a minimum of 15 minutes before being weighed. Again, the weighing was done in the buffer room by removing no more than six tiles at a time from freezer. After weighing, the tiles with ice droplets were returned to the freezer and allowed to chill for at least 15 minutes before impact testing.

150 μ l water



15 mm x 15 mm x 8mm tile

Figure B1: Water Droplet dosed on tile
















Falling rod ice impact tests

The Laray falling rod apparatus was placed in the freezer, leveled, and allowed to equilibrate for a minimum of 1 hour before impact testing was performed. Each tile was tested individually by placing the tile with ice on the Laray base and visually aligning the droplet with center of the rod. The rod was raised to its starting position. The lever holding the rod was tripped to allow the rod to fall on the tile with ice. The rod was wiped with a dry paper towel and returned to its raised position.

The tile with impacted ice was lifted off the base and any loose ice was removed by holding the tile vertically and lightly tapping the tile twice on the Laray base, which was subsequently wiped with a dry paper towel. The final tile weights were recorded, again by removing no more than six tiles at a time from freezer. Calculations for each tile included ice drop weight, ice drop weight loss, and % ice loss.

APPENDIX C: CONTACT ANGLES, ROLL OFF ANGLES AND MAXIMUM SHEAR STRENGTH RESULTS

Table C1: Contact angles for tiles exposed to E1S and E1SR emulsions

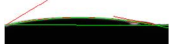














Surface Treatment	Tiles produced with fibers				
	M01	M02	M03	M04	M05
Untreated	 $\Theta = 8.5$ RA= N/A $\Theta_{LY} = --$	 $\Theta = 9.8$ RA= N/A $\Theta_{LY} = --$	 $\Theta = 0.0$ RA= N/A $\Theta_{LY} = --$	 $\Theta = 0.0$ RA= N/A $\Theta_{LY} = --$	 $\Theta = 25.5$ RA= N/A $\Theta_{LY} = --$
E _{1SR}	 $\Theta = 144$ RA= 2.4 $\Theta_{LY} = --$	 $\Theta = 145$ RA= <1.0 $\Theta_{LY} = --$	 $\Theta = 141$ RA= 5.9 $\Theta_{LY} = 166$	 $\Theta = 124$ RA= 7.9 $\Theta_{LY} = 136$	 $\Theta = 133$ RA= 11.7 $\Theta_{LY} = 158$
E _{1S}	 $\Theta = 120$ RA= >90 $\Theta_{LY} = --$	 $\Theta = 119$ RA= 81.2 $\Theta_{LY} = 148$	 $\Theta = 122$ RA= 66 $\Theta_{LY} = 132$	 $\Theta = 128$ RA= 58.5 $\Theta_{LY} = --$	 $\Theta = 129$ RA= 62.4 $\Theta_{LY} = 151$

RA = Roll off angle, deg

Θ = Contact angle, deg (tangent fit average)

Θ_{LY} = Contact angle, deg(Laplace-Young fit)

Table C2: Roll off angles for tiles exposed to E_{1S} and E_{1SR} emulsions

Surface Treatment	Tiles produced without fibers				
	M06	M07	M08	M09	M10
Untreated	 $\Theta = 10$ RA= N/A $\Theta_{LY} = --$	 $\Theta = 14.2$ RA= N/A $\Theta_{LY} = --$	 $\Theta = 5.3$ RA= N/A $\Theta_{LY} = --$	 $\Theta = 0.0$ RA= N/A $\Theta_{LY} = --$	 $\Theta = 0.0$ RA= N/A $\Theta_{LY} = --$
E _{1SR}	 $\Theta = 141$ RA= 4.1 $\Theta_{LY} = --$	 $\Theta = 141$ RA= 7.5 $\Theta_{LY} = --$	 $\Theta = 141$ RA= 4.4 $\Theta_{LY} = 170$	 $\Theta = 141$ RA= 14.4 $\Theta_{LY} = --$	 $\Theta = 136$ RA= 9.1 $\Theta_{LY} = 160$
E _{1S}	 $\Theta = 110$ RA= 56.5 $\Theta_{LY} = 118$	 $\Theta = 109$ RA= 61.3 $\Theta_{LY} = 142$	 $\Theta = 130$ RA= 63 $\Theta_{LY} = 147$	 $\Theta = 124$ RA= 57.6 $\Theta_{LY} = 165$	 $\Theta = 127$ RA= 52.2 $\Theta_{LY} = 145$

RA = Roll off angle, deg

Θ = Contact angle, deg (tangent fit average)

Θ_{LY} = Contact angle, deg(Laplace-Young fit)

Table C3: The correlation between the maximum shear strength and contact or roll-off angle

Specimen ID	Shearing strength, MPa	Contact angle, degrees		Roll off, degrees
		Tangent method	Laplace-Young method	
M1	0.3105	8.5	-	-
M2	0.1842	9.8	-	-
M3	0.2400	0	-	-
M4	0.1847	0	-	-
M5	0.3268	25.5	-	-
M6	0.1821	10.0	-	-
M7	0.2663	14.2	-	-
M8	0.3053	5.3	-	-
M9	0.2811	0	-	-
M10	0.2827	0	-	-
M1 5%	0.1205	143.75	-	2.4
M2 5%	0.0332	145.45	-	<1.0
M3 5%	0.0290	141.4	165.6	5.9
M4 5%	0.0511	123.6	136.3	7.9
M5 5%	0.0484	132.65	158.4	11.7
M6 5%	0.0532	141.45	-	4.1
M7 5%	0.0458	141.05	-	7.5
M8 5%	0.0574	141.35	169.5	4.4
M9 5%	0.0242	140.7	-	14.4
M10 5%	0.0353	136.35	159.6	9.1
M1 25%	0.0611	120.05	127.3	>90.0
M2 25%	0.0474	118.6	148.0	81.2
M3 25%	0.0537	121.65	131.5	66.0
M4 25%	0.0495	128.2	-	58.5
M5 25%	0.0447	129.4	151.4	62.4
M6 25%	0.0347	110.3	117.7	56.5
M7 25%	0.0563	109.1	142.2	61.3
M8 25%	0.0337	129.95	147.2	63.0
M9 25%	0.0742	123.8	135.2	57.6
M10 25%	0.0679	127.05	144.6	52.2



CFIRE

University of Wisconsin-Madison
Department of Civil and Environmental Engineering
1410 Engineering Drive, Room 270
Madison, WI 53706
Phone: 608-263-3175
Fax: 608-263-2512
cfire.wistrans.org

